Palaeogeography, Palaeoclimatology, Palaeoecology 643 (2024) 112180

Contents lists available at ScienceDirect

Palaeogeography, Palaeoclimatology, Palaeoecology

journal homepage: www.elsevier.com/locate/palaeo

Vegetation response to climate change during an Early Jurassic hyperthermal event (Jenkyns Event) from Northern China (Ordos Basin)

Viktória Baranyi [a,*], Xin Jin [b], Jacopo Dal Corso [c], Binbing Li [b], David B. Kemp [c,d]

[a] Department of Geology, Croatian Geological Survey, Sachsova 2, 10000 Zagreb, Croatia
[b] State Key Laboratory of Oil and Gas Reservoir Geology and Exploitation & Institute of Sedimentary Geology, Chengdu University of Technology, Chengdu 610059, China
[c] State Key Laboratory of Biogeology and Environmental Geology, China University of Geosciences, Wuhan 430074, China
[d] Hubei Key Laboratory of Critical Zone Evolution, School of Earth Sciences, China University of Geosciences, Wuhan 430074, China

ARTICLE INFO

Editor: Dr. Bing Shen

Keywords:
Jenkyns Event
Hyperthermal
Palynology
Climate
Vegetation change
Ordos Basin

ABSTRACT

The Early Jurassic Jenkyns Event (or Toarcian Oceanic Anoxic Event T-OAE) was an episode of global warming and C-cycle perturbation that affected both marine and terrestrial ecosystems, but the interplay between climate change and vegetation is not established in detail from sections outside of Europe. Here, abundance changes in spore-pollen assemblages from the lacustrine Anya succession in the Ordos Basin (North China) reveal a unique record of vegetation dynamics during the Jenkyns Event. Plant communities responded to the event with biodiversity losses and the reorganization of gymnosperm-dominated forests. Community-level shifts are observed from the Pliensbachian–Toarcian boundary, but the onset of the negative carbon excursion (NCIE) that marks the event is coeval with the most significant turnover: a switch from a high-diversity vegetation with conifers, seed ferns, cycads, bennettites and ferns to drought-adapted low-diversity flora with Cheirolepidiaceae. The demise of forests and lowland mire biomes resulted in deforestation with increased weathering and soil erosion that exacerbated the terrestrial ecosystem crisis already under stress from rising temperatures. Terrestrial recovery was initiated before the end of the Jenkyns Event with the resurgence of pioneer ferns and lycopsids that colonized disturbed habitats. Plant assemblages signal aridification at the onset of the event with frequent climatic oscillations and extreme weather patterns during the event itself. The main NCIE phase was preceded by a short-lived cooling phase in the earliest Toarcian. In the aftermath of the NCIE, Cheirolepidiaceae forests declined and a more stable biome developed with seed ferns and various conifers. This was contemporaneous with delta development and shallowing of the lake surrounded by lowland mires with ferns, clubmosses and horsetails. Comparison of floral patterns across the Jenkyns Event show that, although Cheirolepidiaceae dominated the event globally, there were differences in vegetation response between coastal and inland areas, and recovery patterns might differ regionally.

1. Introduction

Mesozoic hyperthermal events such as the Jenkyns Event (Müller et al., 2017; Reolid et al., 2020), also known as the Toarcian Oceanic Anoxic Event (T-OAE, ~183 Ma), provide examples from deep time on how marine and terrestrial ecosystems respond to geologically rapid warming (e.g., Zhang et al., 2023a). The Jenkyns Event was coincident with a significant global C-cycle perturbation and a cascade of environmental changes such as global warming (Bailey et al., 2003; Ruebsam et al., 2020a; Ullmann et al., 2020), a rapid increase of atmospheric pCO_2 (up to 1200 ± 400 ppmv; e.g., McElwain et al., 2005; Ruebsam et al., 2020b), increased storminess (Krencker et al., 2015), changes in wildfire activity (Hesselbo et al., 2000; Baker et al., 2017; Qiu et al., 2023), and enhanced chemical weathering (Dera et al., 2009). The climatic instability during the Jenkyns Event was driven by injection of isotopically light carbon into the exogenic C-cycle, as evidenced by a globally synchronous negative carbon isotope excursion (NCIE) (Jenkyns, 1988, 2010) that may have lasted for up to ~1200 kyr (e.g., Suan et al., 2008; Boulila et al., 2019; Ruebsam et al., 2023). The environmental perturbations have been attributed to the emplacement of the Karoo and/or Ferrar Large Igneous Provinces (Pálfy and Smith, 2000; McElwain et al., 2005), orbitally paced CH_4 emissions from marine gas

* Corresponding author.
E-mail address: vbaranyi@hgi-cgs.hr (V. Baranyi).

https://doi.org/10.1016/j.palaeo.2024.112180
Received 20 December 2023; Received in revised form 27 March 2024; Accepted 31 March 2024
Available online 3 April 2024
0031-0182/© 2024 Elsevier B.V. All rights reserved.

hydrates (Hesselbo et al., 2000; Kemp et al., 2005), permafrost thawing (e.g., Ruebsam et al., 2019) or massive decomposition of terrestrial organic matter (Pieńkowski et al., 2016; Them et al., 2019).

The event not only precipitated a substantial decline/turnover of marine biota (e.g., Little and Benton, 1995; Caruthers et al., 2013) but also induced marked changes in terrestrial ecosystems (Pieńkowski et al., 2016; Slater et al., 2019; Reolid et al., 2022). Prominently, high heavy metal loadings from volcanism and terrestrial recycling (Them et al., 2019; Jin et al., 2022) may have poisoned both marine and terrestrial ecosystems (Baranyi et al., 2023). Mutagenic changes in land plants from heavy metal toxicity are evidenced by the presence of aberrant spore-pollen morphologies signalling reproductive stress and decreased fitness in several plant groups during the Jenkyns Event (Baranyi et al., 2023).

Palynology is a key tool for understanding past vegetation, ecosystem and climatic changes (e.g., Birks et al., 2016). The interval of the Jenkyns Event is marked by the globally recorded acme of the thermophilic Cheirolepidiaceae conifers producing *Classopollis* pollen (Fig. 1) and the culmination of a poleward expansion of the tropical Cheirolepidiaceae-biome (Vakhrameyev, 1991; Zakharov et al., 2006; Slater et al., 2019) that began at the Pliensbachian–Toarcian boundary (Vakhrameyev, 1991; Slater et al., 2019). Some work has provided

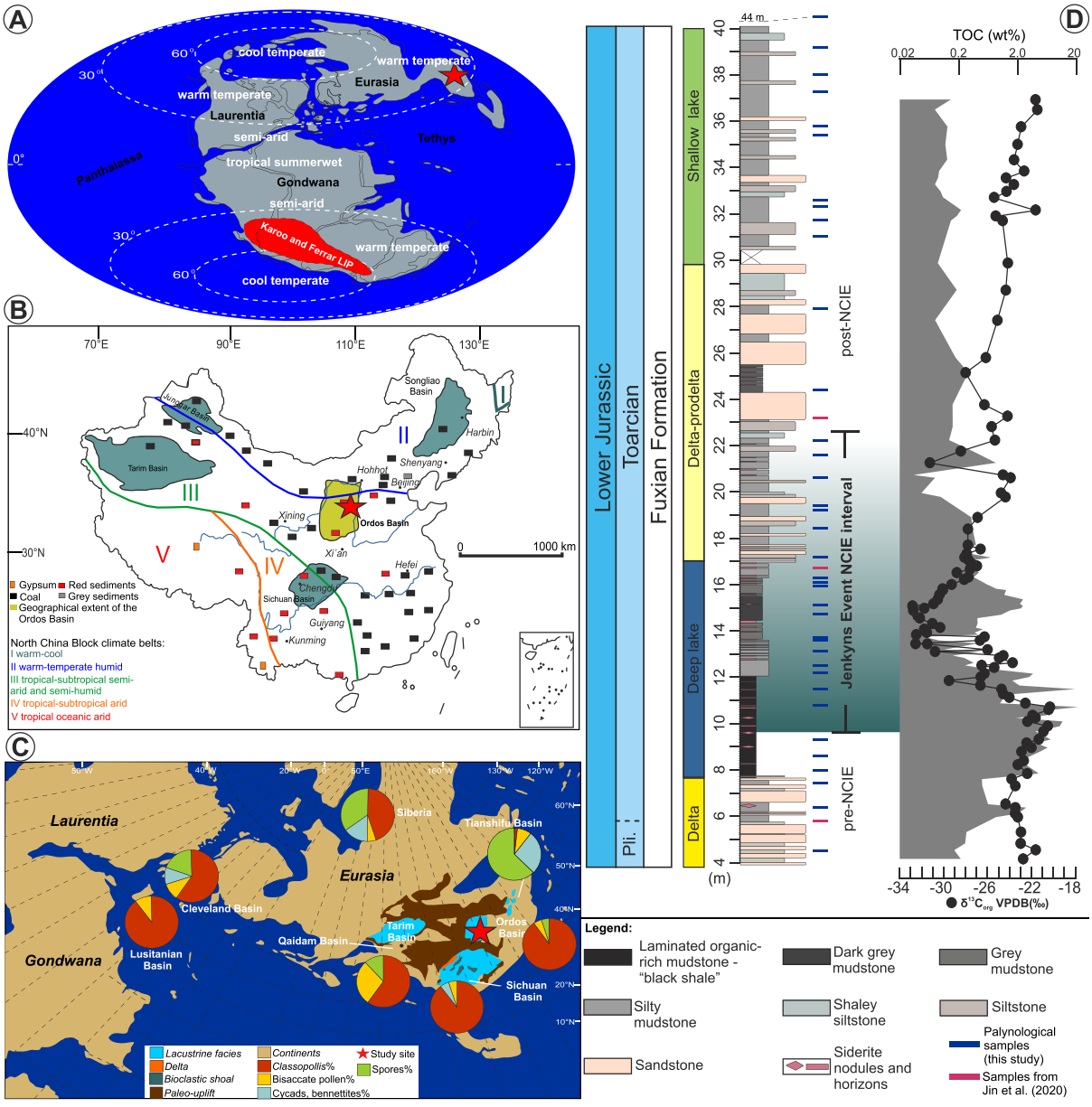

Fig. 1. Geological setting of the Anya section within the Ordos Basin (China) and background climatic conditions on the North China Block during the early Toarcian. A. Early Jurassic paleogeographic reconstruction showing the position of the Karoo and Ferrar Large Igneous Provinces (LIP) in Gondwana and climatic belts after Dera et al. (2009). Redrawn from Font et al. (2022). The location of the Ordos Basin on the North China Block is marked with an asterisk. B. Early Toarcian climate belts in China and associated climate indicators. Modified from Deng et al. (2012, 2017) and Zhang et al. (2020a). The location of the Anya section within the Ordos Basin is marked with an asterisk. C. Characteristic palynological assemblages during the Jenkyns Event NCIE in Eurasia showing the proliferation of *Classopollis*. Data come from Zakharov et al. (2006), Slater et al. (2019), Correia et al. (2018), Wang et al. (2005) and Zhang et al. (2022a) integrated with the present data. Percentage data from Siberia is only an estimate based on the semiquantitative distribution of the palynomorphs assigned to plant groups. Map redrawn from Xu et al. (2017). D. Lithostratigraphy and facies evolution of the Anya succession with the position of the palynological samples shown. Redrawn from Li et al. (2023). Organic carbon isotope ($\delta^{13}C_{org}$) and total organic carbon (TOC) variations in the Anya section are from Jin et al. (2020, 2022). *[2-column fitting]*.

palynological data across the Jenkyns Event (Fig. 1) showing a decrease in seed-fern, cycadophyte and pteridophyte abundances, but most existing data are paleogeographically limited to primarily the Western European Tethys (e.g., Bucefalo Palliani, 1997; Bucefalo Palliani and Riding, 1997; Baranyi et al., 2016; Rodrigues et al., 2016; Correia et al., 2018) and epicontinental realms (Pieńkowski et al., 2016; Slater et al., 2019; Galasso et al., 2021, 2022). Records from terrestrial settings where vegetation changes may be best reflected are scarce. As such, Lower Jurassic continental lacustrine successions such as the Anya section in the northern part of the Ordos Basin, China (Jin et al., 2020, 2022; Li et al., 2023) are useful for tracking vegetation changes where the terrestrial palynomorphs are not diluted by marine phytoplankton, and can provide detailed insights into the interplay between plant communities and terrestrial ecological disturbances. Here we present a high-resolution quantitative palynological dataset from the sedimentologically and geochemically well-constrained Anya section (Jin et al., 2020, 2022; Baranyi et al., 2023; Li et al., 2023) in order to track changes in vegetation assemblages across the Jenkyns Event, and reconstruct the effects of climatic and environmental perturbations on land plant communities.

2. Geological background and the Jenkyns Event in the Ordos Basin

The Ordos Basin is located in the western part of the North China Block (Fig. 1) and is the largest Mesozoic coal and inland petroliferous basin in China, with an area of about 320,000 km^2. Except for minor marine deposits in the Early Triassic, continental lacustrine sedimentation prevailed during the entire Mesozoic (Huang et al., 2008). During the Early Jurassic, the Ordos Basin was located at sub-tropical latitudes and formed an endorheic lake system (Cheng et al., 1997; Jin et al., 2020). The Fuxian Formation in the Anya area mainly consists of black shales, silty shales, grey mudstones and quartz sandstones, and is subdivided into six facies types, including an upward shallowing succession with alluvial fan, lakeshore, delta, deep lake, shallow lake and fluvial environments (Fig. 1).

The Anya section at 38° 24′ 00″ N; 110° 11′48″ E (Fig. 1, S1) is located in the northeastern part of the Ordos Basin, 40 km NE of Yulin City. It records a lake expansion followed by delta progradation and a shallowing phase during the latest Pliensbachian–early Toarcian (Ge et al., 1989, 1991; Jin et al., 2020). The palynological assemblage at Anya correlates to the Australasian *Corollina* (*Classopollis*) *torosa* Oppel Zone spanning from the Hettangian to early Toarcian (Reiser and Williams, 1969; Helby et al., 1987) with typical Pliensbachian–Toarcian palynofloral elements e.g., *Ischyosporites variegatus*, *Contignisporites problematicus*, *C. dunrobinensis*, *Kraeuselisporites reissingeri* (see Jin et al., 2020 for detailed palynostratigraphy). Preliminary non-quantitative palynological analysis was performed by Yan (1992) in the Anya area. Plant macrofossils found previously in the Fuxian Formation are represented mainly by ginkgophyte leaves (*Ginkgoites marginatus, Baiera furcatata, Sphenobaiera huangii, S. leptophylla, S. spectabilis*), ferns (*Todites, Coniopteris, Phlebopteris, Hausmannia*), but remains of seed ferns (*Stenopteris dinosaurensis*), Czekanowskiales (*Czekanowskia rigida, C. setacea, C. fuguensis*), and conifers (*Elatocladus, Podozamites*, *Paleoconiferus, Protoconiferus, Pseudopinus piceites*) were also recorded (Huang and Zhou, 1980; Ge et al., 1989). However, these remains have not been studied extensively.

A broad NCIE is recorded in the Fuxian Formation at the Anya section, spanning from 9.6 m to 22.6 m, across a transition from black shales to dark grey mudstones (Jin et al., 2020, 2022). This NCIE correlates with the globally synchronized Jenkyns Event carbon cycle perturbation, as corroborated by the palynostratigraphical assignment of the section (Jin et al., 2020). The magnitude of the NCIE in bulk organic matter carbon isotopes ($\delta^{13}C_{org}$) is −12.5‰ and occurs coevally with a − 11.3‰ NCIE in long-chain *n*-alkanes (Jin et al., 2020).

3. Material and methods

A total of 41 samples were studied across a 27 m thick interval of the Anya succession (Fig. 1D). The palynofacies dataset was presented in Jin et al. (2022), and the palynological counts for three samples out of the 41 were shown in Jin et al. (2020). Palynological sample preparation followed the protocol of Moore et al. (1991). For detailed description of laboratory procedure and data production see the Supplementary Material. Local palynological assemblages were distinguished by stratigraphically constrained cluster analysis (CONISS) built in Tilia/TiliaGraph based on datasets of at least 300 counted palynomorphs per sample (Grimm, 1987). The Simpson's Diversity Index (Simpson's Index) was calculated with PAST 4.10 (Hammer et al., 2001). The value of this index ranges from 0 to 1, with higher values denoting more diverse communities where taxa are more evenly represented. For paleovegetation reconstruction, the palynomorphs were categorized according to their known or probable parent plant affinities, which largely depends on the relationship between in situ palynomorph findings and recent analogies from the nearest living relative. A modified Mesozoic Eco-Plant model (Zhang et al., 2020b, 2021) and the Sporomorph Ecogroup model (SEG) of Abbink et al. (2004) was applied for tracking paleoclimate and paleoenvironmental variations from the palynological assemblages. The SEG model identifies habitats and coexisting communities and interprets them in paleoenvironmental context, i.e., sea level and climatic changes (explanation of SEG groups in the Supplementary Material). The Eco-Plant model is an ecogroup classification used in modern vegetation studies that takes into consideration the relations between plants and climatic factors such as water availability, temperature, and light (explanation of ecogroups in the Supplementary Material), and groups palynomorphs into various EPH (effect of humidity) and ETH (effect of temperature) categories (Wang et al., 2005; Zhang et al., 2021).

Multivariate ordination performed on the abundance data of selected spore-pollen taxa is used as a tool for illustrating the relationship between variables (taxa) and hypothetic environmental gradients represented by the axes of the ordination diagrams (Kovach, 1993; Correa-Metrio et al., 2014). Detrended correspondence analysis (DCA) was performed on the Anya spore-pollen abundance dataset using PAST (Hammer et al., 2001). For the data analysis, raw data values were Wisconsin double standardized (Jardine and Harrington, 2008) such that each element was divided by its column maximum and then divided by the row total in order to account for the influence of sample size and to equalize the representation of rare versus very abundant taxa (Zhang et al., 2021).

4. Results

4.1. Preservation and identification of the palynological material

The Anya palynological assemblages contain predominantly terrestrial palynomorphs, spores and pollen grains. A total of 61 taxa are recorded (Table 1), comprising 22 pollen, 30 spore taxa (Figs. 2–4) and three aquatic (marine and freshwater). Six taxa were likely reworked from older sediments (Table 1). Palynological raw counts with the botanical affinity and known/presumed ecological preferences of the taxa are provided in the Supplementary Material (Table S1–S2). Of the 41 studied samples, nine were barren and seven samples yielded <300 palynomorph counts per sample after scanning the entire organic residue.

The palynological assemblages in the majority of the samples are diverse and contain well-preserved translucent pale green, yellow–brown sporomorphs. The spore wall coloration index (SCI Batten, 2002) is 2–5, which indicates low thermal maturity of the organic matter, depending on wall-thickness variations between grains and ornamentation (Figs. 2–3). Notably, the spore-pollen grains from 24.4 m to the top of the section are more heterogenous in pigmentation, with

Table 1
Palynomorph taxa in the Anya section in alphabetical order with full author citation below generic level.

Spores
Acanthotriletes midwayensis Pocock, 1964
Calamospora tener (Leschik,1955) Mädler, 1964
Camarazonosporites rudis (Leschik, 1955) Klaus, 1960
Cibotiumspora jurienensis (Balme, 1957) Filatoff, 1975
Cingutriletes sp.
Concavisporites toralis (Leschik, 1955) Nilsson, 1958
Contignisporites dunrobinensis (Couper, 1958) Schulz, 1967
Contignisporites problematicus (Couper, 1958) Döring, 1965
Converrucosisporites sp.
Cyathidites australis Couper, 1953
Cyathidites mesozoicus (Thiergart, 1949) Potonié, 1955
Cyathidites minor Couper, 1953
Deltoidospora sp.
Dictyophyllidites harrisii Couper, 1958
Gleicheniidites conflexus Voronova, 1971
Ischysoporites variegatus (Couper, 1958) Schulz, 1967
Kraeuselisporites cooksonae (Klaus, 1960) Dettman, 1963
Kraeuselisporites reissingeri (Harris, 1957) Morbey, 1975
Leptolepidites verrucatus Couper, 1953
Lunzisporites sp.
Lycopodiumsporites sp.
Manumia delcourtii (Pocock, 1970) Dybkjær, 1991
Neoraistrickia taylorii Playford et Dettmann, 1965
Osmundacidites elegans Xu, 1980
Osmundacidites wellmanii Couper, 1953
Taurocusporites verrucatus Schulz, 1967
Todisporites major Couper, 1958
Todisporites minor Couper, 1958
Toroisporites minoris (Nakoman, 1966) Sun et He, 1980
Uvaesporites argentaeformis (Bolkhovitina, 1953) Schulz, 1967

Pollen grains
Alisporites parvus de Jersey, 1962
Alisporites pergrandis (Bolkhovitina, 1956) Ilyina, 1985
Alisporites robustus Nilsson, 1958
Araucariacites australis Cookson, 1947
Chasmatosporites apertus (Rogalska, 1954) Nilsson, 1958
Chasmatosporites hians Nilsson, 1958
Chasmatosporites oblongus Shang & Li, 1992
Classopollis annulatus (Verbitzkaja, 1962) Li, 1974
Classopollis qiyangensis Shang, 1982
Cycadopites nitidus (Balme, 1957) de Jersey, 1964
Cycadopites typicus Pocock, 1970
Gingkocycadophytus sp.
Monosulcites minimus Cookson, 1947
Perinopollenites elatoides Couper, 1958
Pityosporites scaurus (Nilsson, 1958) Schulz, 1967
Platysaccus queenslandi de Jersey, 1962
Podocarpidites sp.
Protopinus sp.
Quadraeculina anellaeformis Maljavkina, 1949
Sciadopityspollenites macroverrucosus (Nilsson, 1958) Schulz, 1967 emend. Gravendyck, 2023
Sciadopityspollenites thiergartii Schulz, 1967 emend. Gravendyck, 2023
Vitreisporites pallidus Nilsson, 1958

Reworked taxa
Acanthotriletes conicus? Li, 1974
Conbaculatisporites sp
Dictyotriletes sp.
Retitriletes sp.
Schopfites claviger? Sullivan, 1968 emend. Higgs, Clayton & Keegan, 1988
Tigrisporites sp.

Aquatic palynomorphs
Botryococcus braunii Kützing, 1849
Circulisporites sp. (*Concentricystis,* Euglenophyceae)
Micrhystridium sp.

Fungal remains
Diktyothalakos sp.

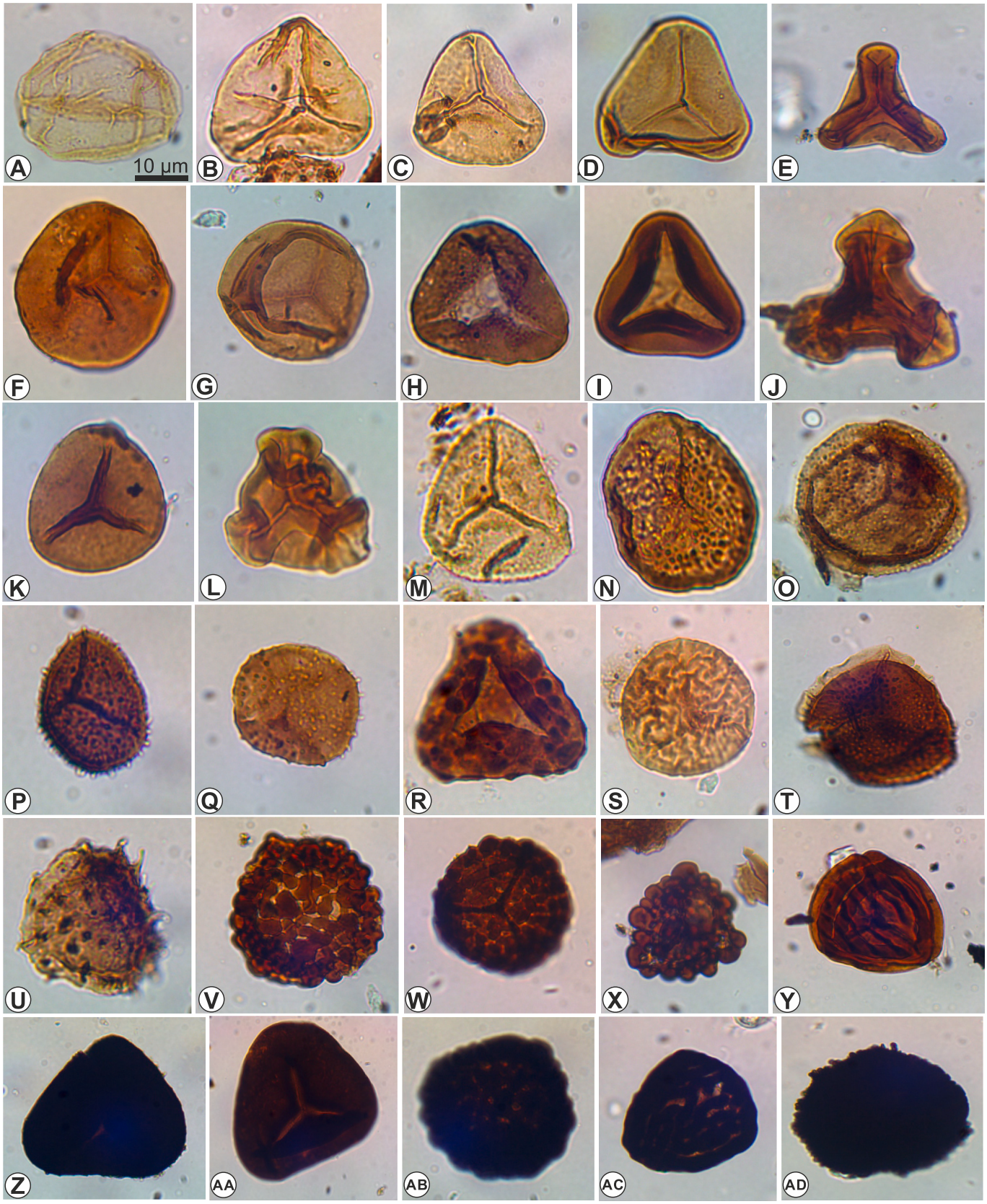

(caption on next page)

Fig. 2. Selected spores from the Anya section. The scale bar in (A) represents 10 μm and refers to each photomicrograph. For full author citation below generic level see Table 1. A. *Calamospora tener* AY65/slide 1, 31.7 m. B. *Dictyophyllidites harrisii* AY29/slide 3, 16.7 m. C. *Deltoidospora* sp. AY21/slide 1, 13.7 m. D. *Deltoidospora* sp. AY42/slide 1, 21.1 m. E. *Concavisporites toralis* NAY76/slide 1, 12.5 m. F. *Todisporites minor* AY29/slide 1, 16.7 m. G. *Todisporites minor* NAY76/slide 1, 12.5 m. H. *Cyathidites australis* AY53/slide 1, 24.4 m. I. *Cyathidites mesozoicus* AY58/slide 1, 28.0 m. J. *Gleicheniidites conflexus* AY17/slide 1, 12.2 m. K. *Toroisporites minoris* NAY76/slide 1, 12.5 m. L. *Cibotiumspora jurienensis* AY06/slide 1, 16.7 m. M. *Lunzisporites* sp. AY21/slide 1, 13.7 m. N. *Taurocusporites verrucatus* AY29/slide 4, 16.7 m. O. *Osmundacidites wellmanii* AY14/slide 1, 9.3 m. P. *Acanthotriletes midwayensis* AY42/slide 1, 21.1 m. Q. *Osmundacidites elegans* AY34/slide 1, 18.4 m. R. *Manumia delcourtii* NAY104/slide 1, 15.1 m. S. *Camarazonosporites rudis* NAY88/slide 1, 13.6 m. T. *Kraeuselisporites cooksonae* AY42/slide 1, 21.1 m. U. *Kraeuselisporites reissingeri,* AY17/slide 1, 12.2 m. V. *Ischyosporites variegatus* AY28/slide 1, 16.3 m. W. *Ischyosporites variegatus* AY44/slide 1, 21.6 m. X. *Uvaesporites argentaeformis* AY31/slide 1, 17.2 m. Y. *Contignisporites porblematicus* AY17/slide 1, 12.2 m. Z. Darkened *Conbaculatisporites* sp. AY53/slide 1, 24.4 m. AA. Darkened *Cyathidites australis*, AY65/slide 1, 31.7 m. AB. Darkened *Ischyosporites variegatus* AY53/slide 1, 24.4 m. AC. Darkened *Contignisporites porblematicus* AY65/slide 1, 31.7 m. AD. *Schopfites claviger*? (reworked) AY65/slide 1, 31.7 m. *[2-column fitting]*.

lighter-coloured and more pigmented specimens with darkened sporoderm (Fig. 2) with dark brown or black colour (SCI 6–7). Darkened and pale-coloured taxa are often identical in terms of taxonomy, but some of the dark-walled palynomorphs e.g., *Acanthotriletes conicus*?, *Schopfites claviger*?, are reworked from Triassic or Palaeozoic strata (Fig. S2).

Aquatic palynomorphs, e.g., freshwater algae *Botryococcus braunii* and *Circulisporites* sp. (Euglenophyceae, see van de Schootbrugge et al., 2024), are extremely rare (Fig. 4). Rare specimens belonging to the acritarch genus *Micrhystridium* are recorded at three horizons during the NCIE (13.1 m, 13.6 m and 15.9 m) which could have been redeposited, or arrived with far-travelled aeolian dust (Glennie and Evans, 1976). Their significance cannot be established due to their low abundance.

4.2. Major palynofloral trends

The stratigraphically constrained cluster analysis distinguishes four informal local palynological assemblages presented in the CONISS dendrogram (Figs. 4–5). The *Alisporites-Chasmatosporites-Deltoidospora* Assemblage (Figs. 4–5) includes the samples from the base of the Anya section to 7.4 m (prior to the NCIE), and is characterized by a roughly equal abundance of spores and gymnosperm pollen. About 50% of the counts belong to the fern spores *Deltoidospora* sp., *Cyathidites* (*C. mesozoicus, C. minor*) and *Dictyophyllidites harrissii*. Gymnosperms are represented by Cheirolepidiaceae pollen, *Classopollis annulatus* (30–40%), *Alisporites* such as *Alisporites parvus, A. pergrandis,* and *A. robustus* (~20% in total) belonging to seed ferns, and pollen of the Bennettitales (*Chasmatosporites*) making up ~5% of the palynological counts.

The interval between 8.3 m to 9.0 m is assigned to the *Perinopollenites* Assemblage (Figs. 4–5) and is characterized by low *Classopollis* abundance relative to a rise in other gymnosperm groups. The proportion of seed fern pollen reaches ~30%, the proportion of bennettite pollen doubles from ~5% to ~10%, and the relative abundance of Cupressaceae-Taxodiaceae related pollen, *Perinopollenites elatoides*, rises from virtually zero to ~10% of the total spore-pollen sum. This pre-NCIE interval has high Simpson's Index values, suggesting high diversity and an even representation of various taxa in the palynological assemblages.

The NCIE interval (9.6 to 22.6 m) is characterized by a decrease in the Simpson's Index due to *Classopollis* superabundance, as species of this genus represent 40–90% of the palynological counts (Figs. 4–5). Two assemblages are distinguished across the NCIE interval: a *Classopollis* dominated assemblage (10.8–16.7 m), and a *Classopollis-Ischyosporites* Assemblage (17.2–23.1 m) (Figs. 4–5). In the *Classopollis* Assemblage, the abundance of most plant groups decreases or they temporally disappear. The proportion of spores *Deltoidospora* sp. and *Dictyophyllidites harrissii* is around 10%, with one exceptional peak of ~40% at 12.2 m (Figs. 4–5). The main difference between the *Classopollis* and *Classopollis-Ischyosporites* Assemblage is the rise in the proportions of the Schizaceae fern spore *Ischyosporites variegatus* and lycopsid spore *Leptolepidites.* In the case of these spore types, the abundance rises from only a few specimens per sample up to 20% of the spore-pollen sum. Smaller Simpson's Index peaks in the *Classopollis*-dominated interval are linked to the appearance of lycopsid taxa and *Ischyosporites*.

The topmost part of the section (above the NCIE) is designated as the *Alisporites-Deltoidospora* local assemblage (24.4–31.7 m) (Figs. 4–5). The increasing trend of the Simpson's Index indicates higher diversity due to the reappearance of bennettitalean, cycadalean, seed fern, Cupressaceae-related pollen, and fern spores. Seed fern related pollen (*Alisporites*) reach their maximum abundance in the section (~40%) at 28.0 m followed by a drastic drop. Coeval with the rise in *Alisporites*, the relative abundance of both the Pinaceae (*Protopinus, Pityosporites*) and Podocarpaceae pollen (*Podocarpidites, Platysaccus queenslandi, Quadraeculina anellaeformis*) increases from <5% to ~10%, together comprising up to 22% of the spore-pollen sum. In the uppermost part of the section above 23.1 m, *Classopollis* pollen strongly decreases then completely disappears, and the palynological assemblage is dominated by the spores of Dicksoniaceae, Cyatheaceae, Matoniaceae, Dipteridaceae, Osmundaceae, Schizaceae ferns and clubmosses.

4.3. Eco-Plant Group (EPG) and Sporomorph Ecogroup (SEG) distributions

Due to the high relative abundances of the Cheirolepidiaceae and Cycadales-Bennettitales in the Anya dispersed sporomorph assemblages, megathermic plants (i.e., plants that tolerate high temperature, inhabiting tropical and subtropical climatic zones) represent the dominant Eco-Plant group (up to 98% of the spore-pollen sum), with moderate contribution from eurythermic ferns (~20%) that dominate the uppermost interval at 24.4–31.7 m (up to 53%) (Fig. 6). Mesothermic plants (i.e., plants living in warm temperate zones), which are represented by the Corystospermales (*Alisporites* spp.), are less abundant with elevated values (~7–27%) only before the NCIE at 5.8–9.3 m and after the NCIE (up to 51% of the total spore-pollen sum). Microthermic plants (i.e., plants inhabiting cooler temperate or subarctic zones; Podocarpaceae, Pinaceae conifers) are subordinate prior to the NCIE (average 3%) with increases (~4–7%) at 8.0–9.3 m followed by a drop to even lower values during the NCIE (~1–3%). However, in the post-NCIE interval the relative abundance of mesothermic and microthermic plants increases to 10–20% of the spore-pollen sum with a maximum of 73% at 28.0 m (Fig. 6).

Considering the effect of humidity (EPH), the majority of gymnosperm taxa (e.g., Cycadales, Bennettitales, Corystospermales, Pinaceae, Podocarpaceae) belong to the mesophytes together with several fern groups (Dicksoniaceae, Cyatheaceae, Dipteridaceae, Matoniaceae, Schizaceae), forming an average of 65% of the spore-pollen sum prior to the NCIE, dropping to ~23% (average) during the NCIE, and going back up to ~42% of the spore-pollen sum after the NCIE (Fig. 6). Xerophyte peaks (up to ~80%) are recorded during the NCIE and are linked to the high abundance of the Cheirolepidiaceae conifers, but their abundance drops to zero coeval with the disappearance of *Classopollis* pollen in the uppermost part of the Anya section (Fig. 6). Hygrophyte plants represented by horsetails, lycopsids and Caytoniales, attain <5% abundance before and during the NCIE, but their abundance reaches 7–16% after the NCIE.

In the Eco-Plant model, euryphytes from the Anya section include several lycopsid and fern taxa (e.g., Pteridaceae) and the Cupressaceae represented by *Perinopollenites elatoides*. Their average abundance is

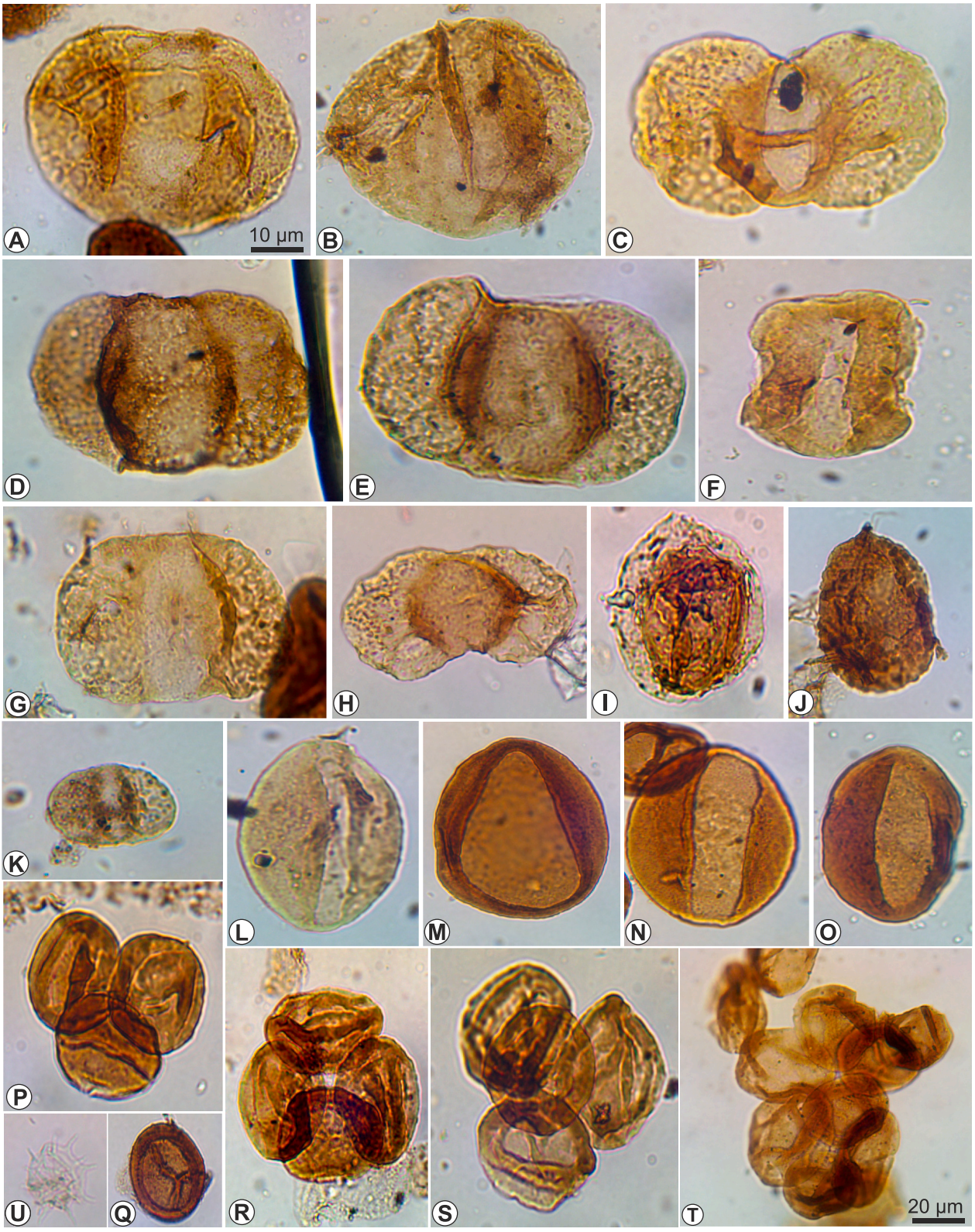

Fig. 3. Selected gymnosperm pollen (conifer, seed fern, cycad and Bennettitalean pollen) and acritarchs from the Anya section. The scale bar in (A) represents 10 µm and refers to each photomicrograph unless otherwise indicated. For full author citation below generic level see the Table 1. A. *Alisporites pergrandis* AY14/slide 1, 9.3 m. B. *Alisporites pergrandis* AY14/slide 1, 9.3 m. C. *Platysaccus* sp. AY34/slide 1, 18.4 m. D. *Alisporites robustus* AY58/slide 1, 28.0 m. E. *Alisporites robustus* AY53/slide 1, 24.4. m. F. *Quadraeculina anellaeformis* AY40/slide 1, 20.6 m. G. *Alisporites parvus* NAY81/slide 1, 13.1 m. H. *Podocarpidites* sp. AY29/slide 1, 16.7 m. I. *Perinopollenies elatoides* AY21/slide 1, 13.7 m. J. *Sciadopityspollenites thiergartii* AY31/slide 1, 17.2 m. K. *Vitreisporites pallidus* AY17/slide 1, 12.2 m. L. *Cycadopites nitidus* NAY66/slide 1, 11.5 m. M. *Chasmatosporites apertus* AY44/slide 1, 21.6 m. N. *Chasmatosporites oblongus* AY44/slide 1, 21.6 m. O. *Chasmatosporites hians* AY44/slide 1, 21.6 m. P. *Classopollis annulatus* triad AY21/slide 1, 13.7 m. Q. *Classopollis qiyangensis* AY21/slide 1, 13.7 m. R. *Classopollis annulatus* tetrad AY21/slide 1, 13.7 m. S. *Classopollis annulatus* tetrad AY21/slide 1, 13.7 m. T. *Classopollis annulatus* agglomerate AY46/slide 3, 22.2 m. Scale bar is 20 µm. U. *Micrhystridium* sp. NAY88/slide 1, 13.6 m. *[2-column fitting]*.

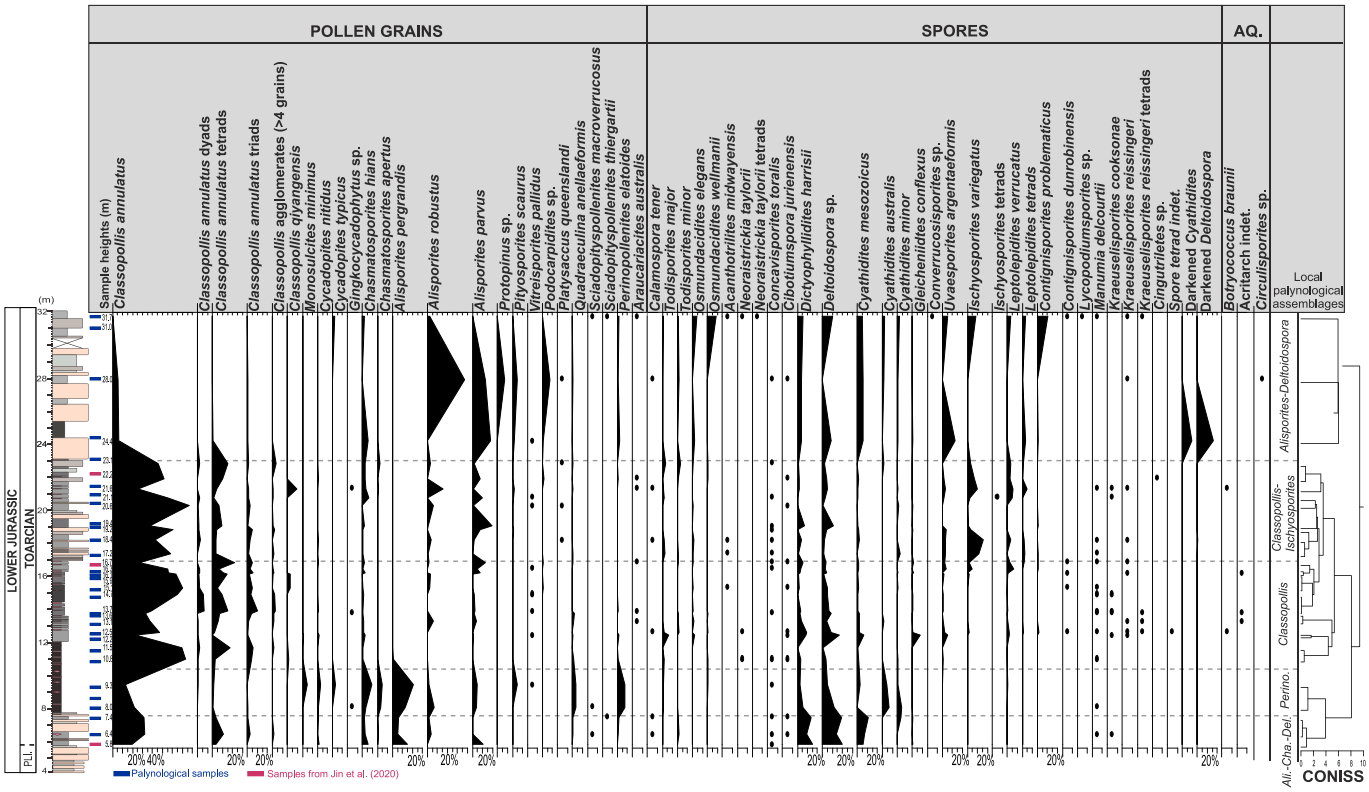

Fig. 4. Quantitative distribution of spore-pollen taxa and aquatic palynomorphs (AQ.) in the Anya section. Palynomorph abundance values are presented as percentage proportions (%) of the total spore-pollen sum. For rare taxa (abundance less <5 counts per sample) only presence-absence data are shown (black circles). *Alisporites-Chasmatosporites-Deltoidospora* Assemblage (Ali-Cha-Del), *Perinopollenites Assemblage* (Perino) in the lower segment. Pli., Pliensbachian. For lithological legend and sample positions the reader is referred to Fig. 1. *[2-column fitting]*.

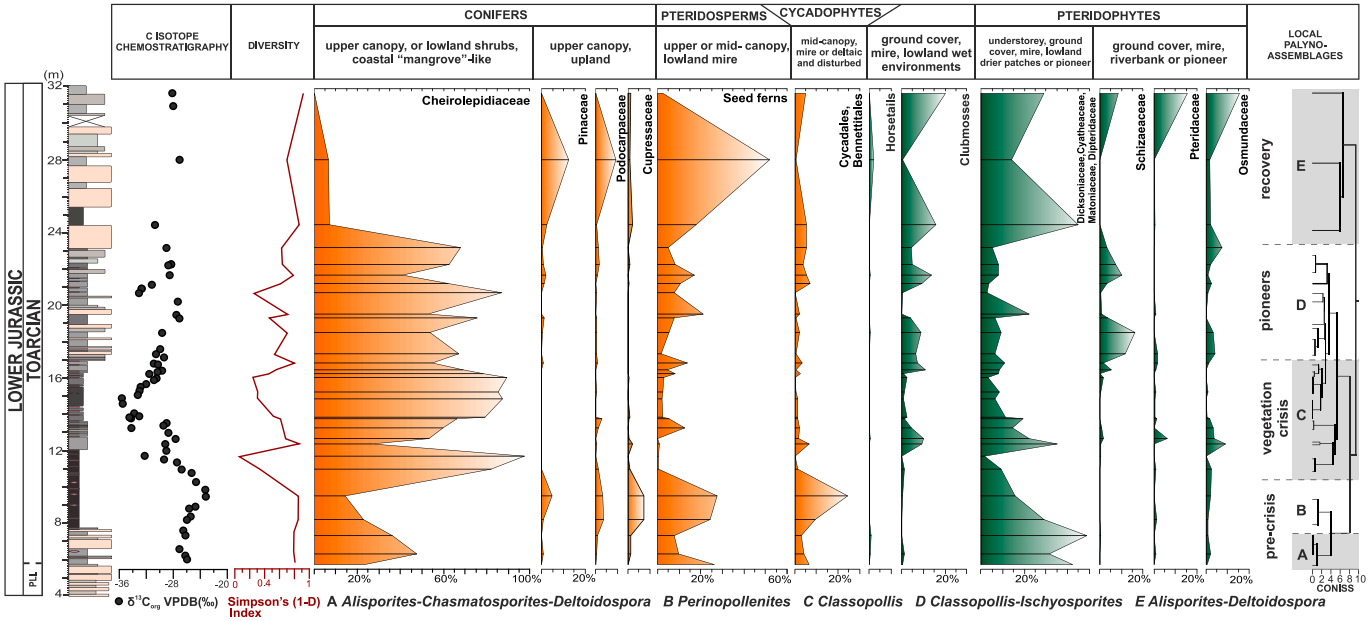

Fig. 5. Vegetation history and biodiversity variations during the Jenkyns Event based on palynological analysis of the Anya section. Abundance variation within plant groups are shown as the percentage proportion changes of certain sporomorph taxa assigned to their known or presumed botanical groups and ecological categories (see Table S2). $\delta^{13}C_{org}$ data are from Jin et al. (2020, 2022). Pli., Pliensbachian. For lithological legend and sample positions the reader is referred to Fig. 1. *[2-column fitting]*.

4–5% with, peaks of 11–16% during the NCIE. Their relative abundance rises in the post-NCIE interval (Fig. 6).

The Sporomorph Ecogroup analysis (Abbink et al., 2004) takes into consideration the habitat and ecological preferences of the dispersed spore-pollen taxa based on the known or presumed botanical affinity of the parent plant. We consider the assignment of *Classopollis* and

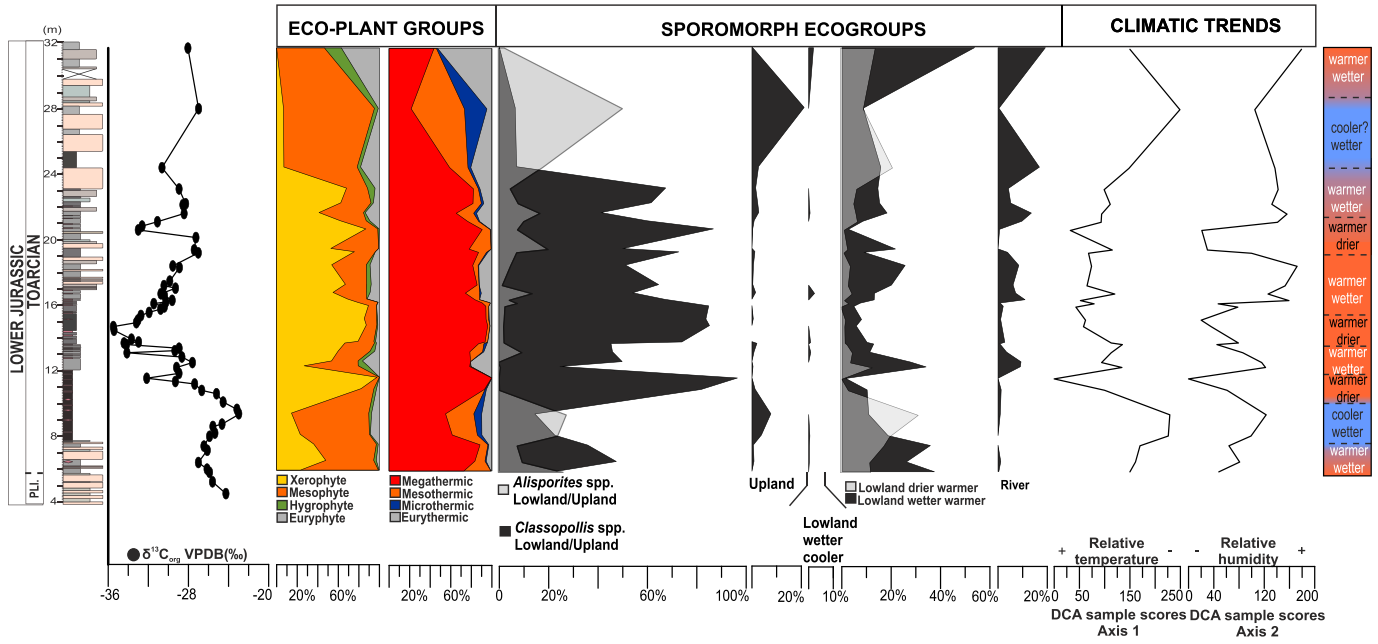

Fig. 6. Distribution of Eco-Plant groups and Spromorph Ecogroups (SEG) in the Anya section expressed as the relative percentage proportion of the total spores-pollen sum together with the sample scores of the DCA plotted against the $\delta^{13}C_{org}$ curves (Jin et al., 2020, 2022) and lithological log depicting the climatic implications of the palynological assemblages. Pli., Pliensbachian. For lithological legend and sample positions the reader is referred to Fig. 1. *[2-column fitting].*

Alisporites to one single ecogroup problematic as they can be placed in both lowland and/or upland/hinterland settings (Fig. 6). Alete bisaccate pollen grains like *Alisporites* spp. were assigned to the upland/hinterland SEG (Abbink et al., 2004; Paterson et al., 2016) with the exception of *A. thomasii* and *Vitreisporites pallidus*. *Classopollis* produced by Cheirolepidiaceae is either not assigned, placed in the coastal SEG (Abbink et al., 2004), lowland SEG (Li et al., 2020a), or upland/hinterland SEG (Paterson et al., 2016). Therefore, these two groups are plotted separately from the remaining SEG categories. Wet lowland and river SEG elements are more abundant prior to and after the NCIE, with additional intervals of increased relative abundances compared to dry lowland SEG elements at 12.2–12.5 m and 17.0–20.0 m (Fig. 6).

4.4. DCA results

Multivariate ordinations are routinely performed on fossil pollen data to visualize changes in plant communities (e.g., Birks, 1986; Baranyi et al., 2016; Li et al., 2020a). However, the nonlinearity of species

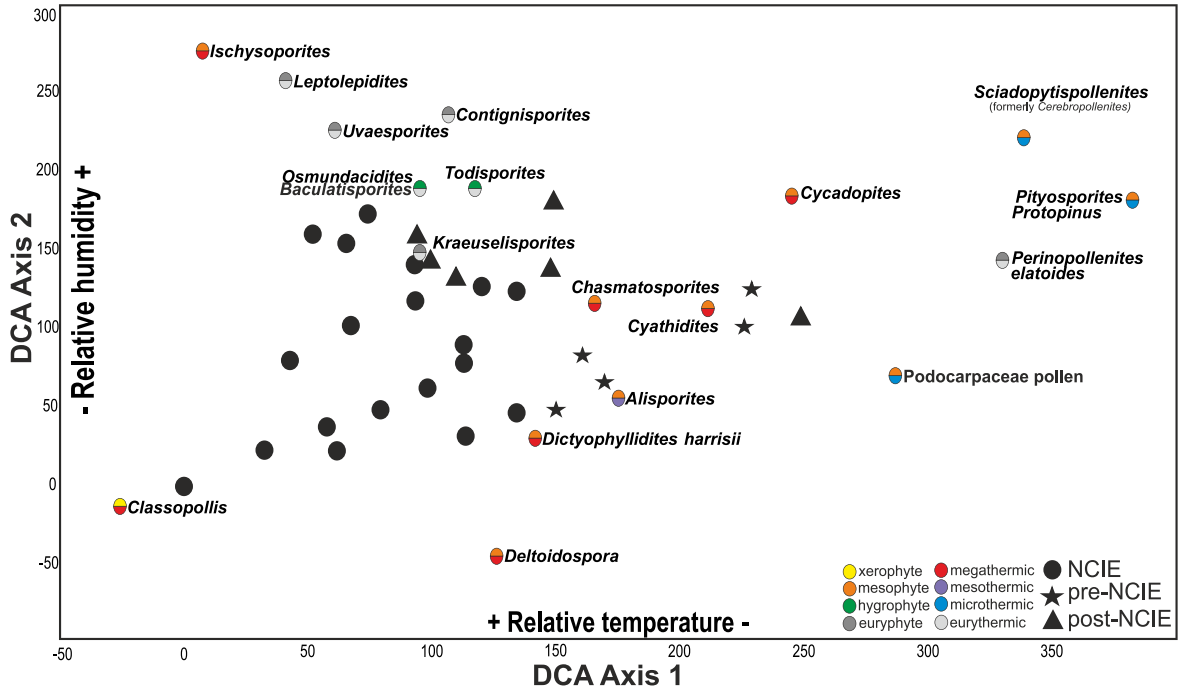

Fig. 7. Detrended correspondence analysis (DCA) ordination plot of the Anya section palynological samples. For the data set used for plotting the DCA dendrogram, see Tables S4–S5. *[1.5-column fitting].*

distributions along gradients and the presence of unimodal (and nonlinear) responses of species to environmental gradients can lead to unbalanced ordination and therefore strong bias in the identification of these environmental gradients (arch/horseshoe effect, Podani and Miklós, 2002; Correa-Metrio et al., 2014). Detrended correspondence analysis (DCA) reduces this bias through dimensional rescaling produced by other ordinations (Correa-Metrio et al., 2014). DCA axes can be interpreted based on the relative position of taxa and ecological needs (a priori) as environmental gradients or variables. Taxa that prefer more temperate conditions, such as Podocarpaceae pollen, Pinaceae (*Pityosporites, Protopinus,*) and *Sciadopytispollenites* attained high DCA Axis 1 scores, while those with affinity to tropical-subtropical

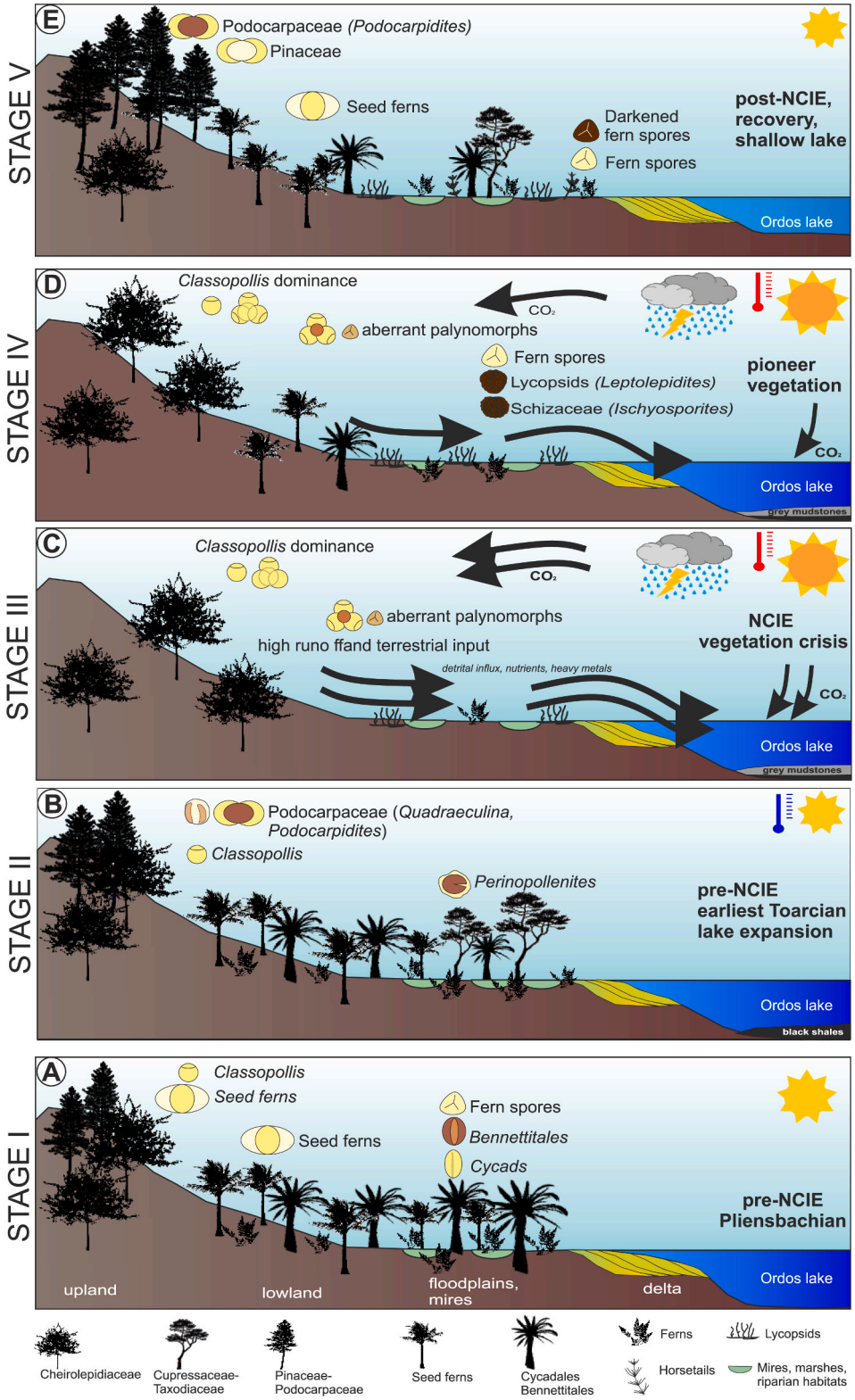

Fig. 8. Schematic reconstruction of the major environmental and climatic changes in the continental ecosystem of the Ordos Basin throughout the Jenkyns Event, with the illustration of characteristic palynomorph and plant types (Stages I—V). See segment 5.1. for explanations. *[1.5-column fitting].*

conditions, like *Classopollis, Ischyosporites* (Schizaceae), *Dictophyllidites* (Dipteridaceae), *Osmundacidites* (*Osmundaceae*), *Cycadopyhtes* and *Chasmatosporites* attained low scores. This axis can thus be interpreted as relative ambient temperature (Fig. 7). On Axis 2, moisture-loving fern taxa (*Todisporites, Contignisporites*, *Osmundacidites*) and lycospid spores (*Uvaesporites, Leptolepidites, Kraeuselisporites*) are ordinated in the upper (more positive) part of the axis (Fig. 7), while cycad-bennettite pollen (*Cycadopites, Chasmatosporites*), seed ferns (*Alisporites*), and ferns spores with transitional hygrophytic-mesophytic affinity are in the middle. *Classopollis* and *Deltoidospora* have lower Axis 2 scores (Fig. 7). DCA sample scores (Figs. 6 and 7) show a clear-cut distinction between the pre-NCIE and NCIE intervals. Axis 1 has high values in the earliest Toarcian and in the aftermath of the NCIE, with smaller oscillations during the main NCIE phase. Axis 2 values are strongly oscillating in the studied section, and become more stable in the post-NCIE. Peaks in Axis 2 sample scores are recorded at 8.0–9.3 m, 12.2–12.5 m, 16.3–19.2 m, and at 21.6 m.

5. Discussion

5.1. Vegetation history during the late Pliensbachian-early Toarcian

The Anya section records a prominent vegetation change, expressed as a temporal drop in the abundance of multiple plant groups during the Jenkyns Event. Vegetation restructuring can be illustrated via division of the Anya section into five stages (I to V, Fig. 8A–E), corresponding to the local informal palynological assemblages (Section 4.2).

5.1.1. Stage I (5.8–7.4 m) Pliensbachian–Toarcian forest and lowland mire ecosystems

Preceding the NCIE, during the Pliensbachian–earliest Toarcian (Fig. 8A), the picture of a high diversity multi-storeyed forest and mire ecosystem emerges from the overall composition of the palynological assemblages, with a well-developed understory of herbaceous ferns and horsetails (Fig. 8). The mid-canopy vegetation was dominated by seed ferns, cycads, bennettites, ginkgophytes, while the upper canopy level was made up of conifers (Cheirolepidiaceae, Podocarpaceae, Cupressaceae). Dicksoniaceae, Cyatheaceae, Matoniaceae, Dipteridaceae and Osmundaceae ferns inhabited the understory and mires. Cycadales and Bennettitales lived in lowland deltaic environments and well-drained soils close to fluvial channel margins, often in disturbed environments (Abbink et al., 2004; Pott, 2014). In the Ordos Basin they most likely lived further from the waterlogged margins (Mussard et al., 1997) in lowland environments somewhat drier than the producers of *Perinopollenites elatoides*, which are of taxodiacean-cupressaceaen affinity and linked to wet habitats (McElwain et al., 2007).

5.1.2. Stage II (8.0–9.3 m) Lake expansion and riparian habitats with Cupressaceae-Taxodiaceae

The rise in *Perinopollenites elatoides* abundance at ~8.0–9.3 m in the earliest Toarcian during Stage II (Fig. 8B) was associated with high primary productivity and black shale deposition in a deep lake environment (Jin et al., 2020; Li et al., 2023). This can be interpreted as an intense phase of lake level rise and the expansion of the riparian and probably swamp environment that was colonized by Cupressaceae-Taxodiaceae producing *Perinopollenites*, cycads, and bennettites (Fig. 8B). The same trends have been observed in the adjacent Sichuan Basin in the early Toarcian prior to the NCIE (Xu et al., 2021), implying that both local and regional factors affected the vegetation patterns in the Ordos Basin.

5.1.3. Stage III (10.8–16.7 m) Vegetation crisis with Cheirolepidiaceae proliferation

Maximum Cheirolepidiaceae abundance at Anya (40–90% of the spore-pollen sum) was reached during Stage III, which was simultaneous with an abrupt fall in the Simpson's Index values indicating environmental disturbances and vegetation crisis, thus promoting the dominance of a few species (e.g., Lindström, 2021). In the Northern Hemisphere, the geographical distribution of Cheirolepidiaceae-pollen (*Classopollis*) significantly expanded to the north in the late Pliensbachian–early Toarcian culminating during the NCIE as a consequence of global warming (Vakhrameyev, 1991; Wang et al., 2005; Zakharov et al., 2006; Pieńkowski et al., 2016; Deng et al., 2017; Correia et al., 2018; Slater et al., 2019; Jin et al., 2020; Zhang et al., 2020a, 2022a; Galasso et al., 2021, 2022). Mesozoic cheirolepids were trees or shrubs in upland or lowland environments that may have populated upland or coastal areas and possibly even mangrove-like habitats (e.g., Watson and Alvin, 1996; Sajjadi and Playford, 2002). Locally, Cheirolepidiaceae can be opportunistic and abundant in a disturbed environments where new habitats became available after mass extinctions or floral turnovers, e.g., after the Cretaceous–Paleogene or the End-Triassic mass extinctions (Barreda et al., 2012; Bonis and Kürschner, 2012; Li et al., 2020a; Lindström, 2021; Zhang et al., 2022b; Bos et al., 2023). They were likely generalists and adapted to a wide range of environments with large ecological flexibility (Axsmith, 2006), and were able to thrive even in the impoverished forest and lowland habitats during the vegetation crisis interval at Anya. Overall, the vegetation data show that plant communities experienced temporal losses in species richness during Stage III, but they did not face complete extirpation and re-occurred after the Jenkyns Event. The event led to the collapse of the structured forest community, i.e., the demise of the mid-canopy elements such as seed ferns and the Cycadales-Bennettitales. Some ferns in the understory of forests develop more successfully in the shade under low-light conditions created by forest canopy or as epiphytes on trees, with only a few taxa that can grow under full sunlight (Sharpe et al., 2010; Olivera et al., 2015). Therefore, the loss of the mid-canopy and changes in the upper-canopy tier likely diminished the ground cover vegetation, leading to deforestation and a shift to a more open landscape (Fig. 8C).

5.1.4. Stage IV (17.2–23.1 m) Pioneers and the onset of the vegetation recovery

During Stage IV, pioneering plant taxa such as Schizaeaceae ferns (*Ischyosporites variegatus*) and lycopsids (*Leptolepidites*) appeared and thrived as early successional plants in the Anya section, accompanied by Dicksoniaceae, Cyatheaceae, Matoniaceae, and Dipteridaceae ferns (Fig. 8D). Their presence in the crisis interval (although subordinate compared to the Cheirolepidiaceae) indicates temporally more favourable conditions that allowed the colonization of vacant ecospaces after the collapse of the tree-forming vegetation. Although ferns in general prefer moist habitats, several fern families were adapted to dry or disturbed high-stress environments (van Konijnenburg-Van Cittert, 2002). The Anya Schizaceae "spore spikes" appear similar to other Mesozoic hyperthermal and extinction events (e.g., van de Schootbrugge et al., 2009; Bonis and Kürschner, 2012; Lindström, 2016, 2021; Gravendyck et al., 2020; Li et al., 2020a; Galasso et al., 2022; Bos et al., 2023), where early successional plant communities with herbaceous ferns and lycopsids colonized depauperate landscapes, while mid-canopy elements were still absent (Fig. 8D).

Sciadopityspollenites (previously named *Cerebropollenites*, see Gravendyck et al., 2023) was another pioneer taxon during the early Toarcian vegetation turnover in the European epicontinental realm (Slater et al., 2019; Galasso et al., 2022). However, unlike in the NW European realm, there is no *Sciadopityspollenites* peak at Anya. Both *S. macroverrucoss* and *S. thiergartii* are rare constituents of the palynological assemblages in the entire Anya section (before, during and after the NCIE) (Table S1). *Sciadopityspollenites* is comparable to the pollen of the modern *Tsuga* (hemlock) or Japanese umbrella-pine, *Sciadopitys verticillata*, and could have been produced by the Miroviaceae conifers, basal Sciadopityaceae (Hofmann et al., 2021) or Taxodiaceae (e.g., Dejax et al., 2007). Modern *Sciadopitys* has only one living species, which is restricted to humid regions of Japan, living on rocky slopes in mixed middle altitude cloud forests at 500–1200 m elevation (Hofmann et al., 2021). In the present

study, *Sciadopityspollenites* is considered to be a more temperate floral element based on its ordination together with microthermic and eurythermic taxa like the Podocarpaceae, Pinaceae and *Perinopollenites* in the DCA. This difference in the palynological composition between the epicontinental realm and the Ordos Basin highlights some variation in the vegetation response due to pre-existing climate gradient and/or regional and local environmental conditions (e.g., topography, orography, distance from the ocean, coastal or inland settings) in general.

5.1.5. Stage V (24.4–31.7 m) Recovery of the forest and lowland mire ecosystems

After the NCIE land plant communities gradually returned to their pre-event diversity, with similar taxonomical composition establishing a more stable biome (Fig. 8E). However, the relative proportion of the plant groups differed in comparison to the pre-NCIE and latest Pliensbachian assemblages. Both Cycadales and Bennettitales remained low in abundance, and the mid-canopy was filled primarily by seed ferns. During the early recovery the upper canopy level was still dominated by the Cheirolepidiaceae but they were subsequently replaced by the Podocarpaceae and Pinaceae, indicating more temperate conditions (Sajjadi and Playford, 2002; Abbink et al., 2004; Olivera et al., 2015; Li et al., 2020a). The large-number of spores belonging to clubmosses, horsetails and ferns at 24.4–31.7 m signals the re-establishment of the herbaceous understory in mire and wet lowland habitats. However, this re-establishment was simultaneous with delta development and shallowing of the lake in the Ordos Basin after the Jenkyns Event interval (Fig. 8E), thus indicating that a combined effect of climatic trends and local depositional changes influenced the vegetation patterns at Anya.

5.2. Climatic changes in the Ordos Basin associated with the Jenkyns Event

The climatic implications of the palynological data are based on the known or presumed ecological affinities of the parent plants, the Eco-Plant group distribution, and the patterns of the DCA scores. Stratigraphical changes in the DCA sample scores provide an approximate picture of how the associated environmental gradient changed through time (Correa-Metrio et al., 2014). High sample scores on Axes 1 and 2 indicate cooler temperate and more humid conditions (Fig. 6). Low axis scores for Axis 1 are linked to rising temperatures while low values on Axis 2 indicate aridity and low moisture levels (Fig. 6). The trend of the sample scores reflects a wet warm late Pliensbachian–earliest Toarcian climate with a drop in humidity at the onset of the NCIE, albeit with some oscillations present in moisture levels with warmer drier and wetter intervals. The climate was likely wetter and cooler in the earliest Toarcian before the NCIE and probably temperate in the post-NCIE interval.

The Ordos Basin was located in a subtropical to warm temperate and humid climatic zone during the Hettangian–Pliensbachian (Deng et al., 2012, 2017), as reflected by the predominance of mesophytic and high abundance of megathermic-mesothermic vegetation components at Anya. During the early Toarcian, increasing abundance of megathermic plants e.g., Cheirolepidiaceae was recorded simultaneously with the NCIE and greenhouse-gas induced warming coeval with a shift to semi-arid and semi-humid climate on the North China Block (Huang and Zhou, 1980; Deng et al., 2012, 2017, 2024). The first rise in Cheirolepidiaceae abundances was recorded in the Northern Hemisphere at the Pliensbachian–Toarcian boundary (Slater et al., 2019), likely

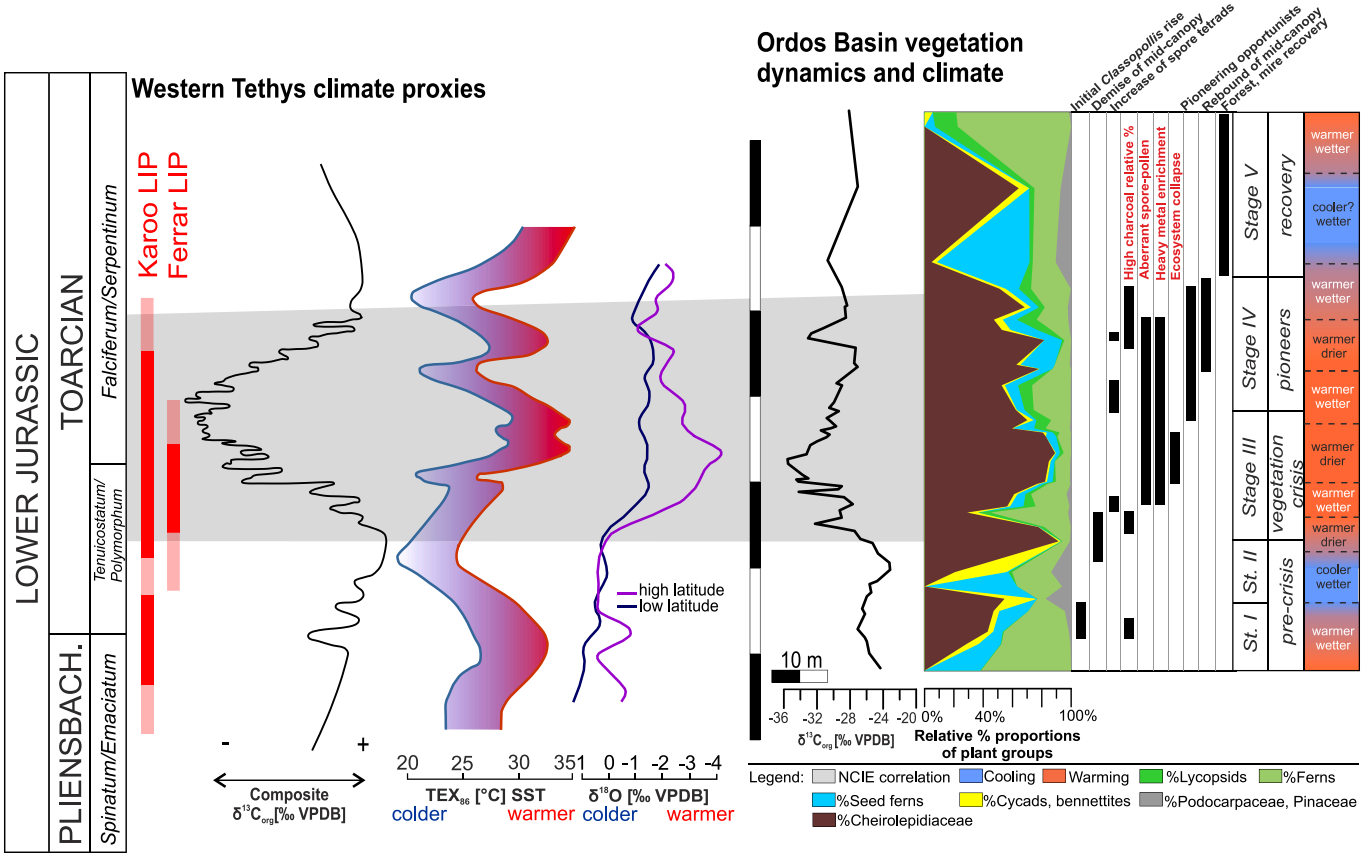

Fig. 9. Correlation of the Anya vegetation dynamics and climate evolution with sea water temperature trends in the Western Tethys and global volcanic events. The Western Tethys composite bulk organic carbon isotope, sea water temperature curves and oxygen isotope data are redrawn after Ruebsam et al. (2019, 2020a) and Ruebsam and Al-Husseini (2020). Age of the Karroo and Ferrar LIP follows the correlation in Ruebsam et al. (2019, 2020a). Data related to charcoal abundances, heavy metal enrichment and spore-pollen teratology in the Anya section is from Jin et al. (2022) and Baranyi et al. (2023). *[2-column fitting]*.

correlating with the first pulses of LIP activity and initial temperature rise (Moulin et al., 2017; Al-Suwaidi et al., 2022). Sea surface temperatures (SST) derived from oxygen isotopes of marine invertebrates (Dera et al., 2011; Korte et al., 2015) and TEX_{86}-based data from the Western Tethys (Ruebsam et al., 2020a) indicate warming (albeit with temperature swings) during the Pliensbachian to early Toarcian (Fig. 9). This warming trend from the Pliensbachian–Toarcian onwards was interrupted by a short-lived cooler interval in the earliest Toarcian (pre-NCIE) linked to the possible development of polar ice (e.g., Suan et al., 2010; Dera et al., 2011; Ruebsam et al., 2019, 2020a; Nordt et al., 2022). This cool snap prior to the negative isotope excursion shows good temporal correlation with the increase in microthermic palynotaxa (Podocarpaceae, Pinaceae), *Perinopollenites* pollen, and a drop in the abundance of thermophilus Cheirolepidiaceae in the Ordos Basin (Fig. 9).

The vast majority of published data on hydroclimate across the Jenkyns Event indicate a shift to a warmer and wetter climate during the event (e.g., Cohen et al., 2004; Dera et al., 2009; Montero-Serrano et al., 2015; Xu et al., 2018; Kemp et al., 2019) yet newly emerging data show that aridification also occurred, especially in inland areas (Vakhrameyev, 1991; Wang et al., 2005; Fantasia et al., 2018; Deng et al., 2024). During the NCIE, continental environments on the North China Block experienced warming and the expansion of the tropical-subtropical semi-arid to semi-humid and tropical oceanic arid climate belts based on the distribution of climate sensitive plant assemblages (Wang et al., 2005; Ashraf et al., 2010; Deng et al., 2012, 2017, 2024; Zhang et al., 2020a, 2022a; Qiu et al., 2023), as well as climate indicative facies such as red beds, calcretes, dolomites, gypsum (e.g., Li et al., 2020b), and the loss of coals (Eberth et al., 2001; Ashraf et al., 2010; Sun et al., 2010; Deng et al., 2012, 2024). The Toarcian flora of the Sangonghe Formation in the Junggar Basin (NW China) contained higher relative percentage (45%) of thermophilus and arid-tolerant taxa e.g., *Marattiopsis asiatica, Phlebopteris, Dictyophyllum* (ferns), *Otozamites-Zamites-Dictyozamites* (bennettites), *Brachyphyllum* (Cheirolpidiaceae), and *Cadmisega ephedroides* (Gnetales) compared to the underlying and overlying beds that contained primarily warm-humid climate indicators in the plant assemblages (Sun et al., 2010; Deng et al., 2024). In particular, the presence of *Ephedra*-related plant fossils (*Cadmisega,* Gnetales) in the late Early Jurassic floras of both the Junggar and Qaidam basins indicate an arid climate and harsh conditions that suggests significant climatic warming and aridification during the early Toarcian (Deng et al., 2024). A similar trend with the rise of thermophilus and arid-tolerant taxa was observed in other inland areas on the North China Block as well e.g., in Central Inner Mongolia, North Hebei (Wang, 2002) and in the Datong Basin (Li and Hu, 1984).

This palaeontological and sedimentological evidence is in line with the results from the General Circulation Model (GCM; Chandler et al., 1992), GENESIS (Peyser and Poulsen, 2008) and Fully coupled Ocean–Atmosphere Model (FOAM; Dera and Donnadieu, 2012) that showed increased continental temperatures with more intense seasonal monsoon and seasonally arid climate in the low to middle latitudes of Panthalassan and Tethyan coasts in a high pCO_2 world. According to these models, warming in continental interiors would be more pronounced than over the sea due to decreased soil moisture and lack of convective precipitation (Peyser and Poulsen, 2008). The extremely high summer temperatures in the continental interior and high land-sea temperature gradient causes the reversal of normal monsoon circulation that draws moisture-laden air producing excessive seasonal rainfalls as flash floods (e.g., Loope et al., 2001; Vollmer et al., 2008). In the Ordos Basin, the early Toarcian C-cycle perturbation was coeval with a pronounced increase in the thermophilous drought-adapted Cheirolepidiaceae conifers that colonized disturbed lowland as well as upland habitats (according to their SEG). Deforestation, open landscape and the proposed seasonal flash floods thus explains the "wash in" of more upland and less water-dependent vegetation elements like *Classopollis* pollen from well-drained slopes to the marine/lacustrine basins (Bonis et al., 2010; Baranyi et al., 2018).

The observations from Anya suggest a shift to drier conditions at the onset of the Jenkyns Event coeval with the falling limb of the $\delta^{13}C_{org}$ curve, but with a more vigorous monsoonal circulation and climatic extremities during the main NCIE phase according to the models of Loope et al. (2001) and Dera and Donnadieu (2012) represented by the oscillation between warmer drier and warmer wetter intervals (Fig. 9). Likely, temporal decreases in Cheirolepidiaceae abundances indicate warm and relatively wetter intervals at Anya (e.g., 12.2–12.5 m, 16.3–19.2 m, and at 21.6 m). The climate in the Ordos Basin after the Jenkyns Event NCIE was probably more temperate, as indicated by the rise of microthermic conifers (mainly Podocarpaceae and Pinaceae conifers) and the disappearance of the thermophilous Cheirolepidiaceae (Fig. 9). Similarly, the decline in Cheirolepidiaceae is also recognized in the Qaidam Basin, where the Aalenian–Bajocian vegetation is mainly represented by fern families, Cyatheaceae and Dicksoniaceae (Wang et al., 2005). After the Jenkyns Event, the accumulation of coals resumed in the Ordos Basin (Li et al., 2019) with mainly Osmundaceae, Dicksoniaceae ferns, Ginkgoales and Czekanowskiales occurring, indicating humid and warm-temperate climate as thermophilic, drought-adapted conifers like the Cheirolepidiaceae were absent (Li et al., 2019; Zhang et al., 2023b).

5.3. Triggers of the terrestrial biotic crisis, adaptations and escape mechanisms

For terrestrial biotic crises, the common suspected causes are climatic extremes (e.g., hot/cold thermal stress, changes in annual precipitation, floods), volcanic winters, acid rain, soil erosion, harmful UV-B radiation, wildfires, and heavy metal pollution leading to immediate or long-term vegetation dieback and habitat destruction (e.g., Bond and Grasby, 2017). Volcanic activity (e.g., Percival et al., 2015), weathering as well as wildfires were likely the main sources of toxic heavy metals (e.g., Hg, Cd, Cr, Cu, Pb, As) in terrestrial ecosystems during hyperthermal events (e.g., Lindström et al., 2019; Them et al., 2019; Chu et al., 2021; Jin et al., 2022). At Anya, the occurrence of teratological spore-pollen morphologies in ferns, clubmosses and conifers (including dwarfed and aberrant spores, aberrant spore tetrads, and aberrant *Classopollis* tetrads) was coeval with higher relative abundances of Hg, Cu, Cd, Cr, Pb, and As at 12–21.7 m within the Jenkyns Event NCIE (9.6–22.6 m) indicating that heavy metal toxicity was likely a primary trigger of vegetation crisis besides climate change (Fig. 9) (Baranyi et al., 2023). Heavy metal toxicity negatively affects the metabolic pathways and gaseous exchange leading to plant growth retardation e.g., root reduction, reduced fitness, and reduced reproductive abilities such as lowered seed and biomass production rate (Nagajyoti et al., 2010). Some of these factors negatively influence the functional role of vegetation in soil stabilization and habitat maintenance (Vannoppen et al., 2017) that consequently led to soil erosion and increased runoff into the Anya lake system (Jin et al., 2022? Baranyi et al., 2023), similar to the End-Permian extinction event (Algeo et al., 2011; Vajda et al., 2020). In the case of the Jenkyns Event at Anya, acceleration of the hydrological cycle is evidenced by increases in weathering proxies (Li et al., 2023), and a synchronous rise in the occurrence of spore tetrads and heavy metal relative abundances at 12.5–13.1 m at the onset of the NCIE (Fig. 9) that was followed by the first peaks of aberrant palynomorphs at 13.2 m (Baranyi et al., 2023). Notably, the decline in the relative abundance of mid-canopy elements (seed ferns, bennettites, cycads) commenced before the occurrence of teratological palynomorphs and the rise in spore tetrads, indicating that they responded earlier to the environmental perturbation compared to ferns, clubmosses or conifers (Fig. 9). It is likely that the shift to warmer and drier conditions at the onset of the NCIE already negatively impacted seed ferns, bennettites and cycads before the release of the heavy metals into the terrestrial ecosystem.

In summary, all aspects of the ongoing climate change and

community-level vegetation turnover at Anya, in particular the switch to *Classopollis*-dominated vegetation from the Pliensbachian–Toarcian boundary onwards, contributed towards the enhanced weathering, runoff and leaching of heavy metals from their inorganic and organic hosts. Higher relative abundance of narrow-leaved plants such as the Cheirolepidiaceae conifers compared to broad-leaved cycads and seed ferns promote flammability and wildfire activity (Belcher et al., 2010; Lindström, 2021). Widespread charcoal abundance data (Baker et al., 2017; Jin et al., 2022) and organic macerals (Xu et al., 2021) suggest increased wildfire activity at the onset of the NCIE, which likely also contributed to the release of heavy metals into the terrestrial ecosystems. The physiological effects of high pCO_2 level decreases stomatal conductance and suppresses plant transpiration resulting in increased runoff (Betts et al., 2007; Franks and Beerling, 2009; Gedney et al., 2006; Steinthorsdottir et al., 2012; McElwain, 2018). In particular, Cheirolepidiaceae have lower maximum stomatal conductance rates (g_{max}) compared to other gymnosperms (and angiosperms) (e.g., Fay, 2014) enhancing continental weathering and runoff (Steinthorsdottir et al., 2012; McElwain, 2018).

The proliferation of Cheirolepidiaceae during the Jenkyns Event NCIE could be explained by the biological adaptation of this group to high stress environments. Thick cuticle and papillate stomata could be efficient tools in water-repellence and self-cleaning during hyperthermals, and protect the plant from stresses such as drought, volcanic ash-fall, excess UV-B radiation and pathogens (Haworth and McElwain, 2008). Polyploidy or whole genome duplication represented by the formation of uneven or large-sized *Classopollis* grains indicative of the presence of multiple chromosome sets has been observed at the End-Triassic (Kürschner et al., 2013; Gravendyck et al., 2020) as well as at the Jenkyns Event (Baranyi et al., 2023). This condition can arguably make the parent plants more tolerant to external environmental stress (Levin, 1983), which may have secured the continued success and ecological resilience of the Cheirolepidiaceae during environmental perturbation (Kürschner et al., 2013; Gravendyck et al., 2020). Nevertheless, currently there is still no consensus about the real presence of a polyploid advantage as many recently formed polyploid species have higher extinction rates in response to recent environmental stress than their diploid relatives (Arrigo and Barker, 2012; Bencha et al., 2022).

Terrestrial palynological data across the Jenkyns Event show that although many plant groups temporally disappeared, they returned to the post-event ecosystems. Migration was likely a key escape mechanism for plants during ancient hyperthermal events (McElwain, 2018). Whilst a continental interior like the Ordos Basin experienced aridification and enhanced seasonality (Deng et al., 2024), parts of the North China Block (in particular its north eastern segment) remained warm and more humid due to the vicinity of the Panthalassa (Deng et al., 2017, 2024; Zhang et al., 2022a). The vegetation there was characterized by the predominance of spores, cycad-bennettites, seed ferns and Pinaceae conifers with lower Cheirolepidiaceae proportions (Liu et al., 2019; Zhang et al., 2020a, 2022a). A similar palaeobotanical trend was observed in the SW Tarim Basin that was near the NE margin of the Tethys during the Early Jurassic (Deng et al., 2024). This regional difference in floral composition, together with the resurgence of the same plant taxa in the recovery period of the Jenkyns Event, suggest that some taxa (in particular seed ferns and cycadopyhtes) prevailed at higher latitudes or in coastal areas while the vegetation in the Ordos Basin experienced a severe vegetation crisis and temporal biodiversity losses.

6. Conclusions

The Anya section in the Ordos Basin is a unique archive of vegetation dynamics and terrestrial ecosystem crisis linked to global warming and global C-cycle perturbation during the early Toarcian. Vegetation data prior to the Jenkyns Event represent a high-diversity forest and lowland mire biome. Based on the quantitative palynological record the vegetation responded with temporal biodiversity losses and reorganization of forest structure during the Jenkyns Event. The proliferation of the thermophilic Cheirolepidiaceae (*Classopollis*) during the NCIE (9.6 to 22.6 m) coincided with the fragmentation and destruction of mid-canopy and understory habitats inferred from low gymnosperm pollen (seed ferns, cycads, bennettites) and low ground cover (ferns, club-mosses, horsetails) abundances. Pioneering plant groups (e.g., Schizaceae ferns, lycopsids) colonized disturbed habitats in the first phase of recovery. A decline of Cheirolepidiaceae abundance after the NCIE coeval with a rise in seed ferns and Podocarpaceae-Pinaceae conifers and ferns signalled the resurgence of a stable forest biome with lush understory and the re-establishment of lowland mire habitats.

On the North China Block, the climate shifted from warm and humid to semi-arid to semi-humid at the onset of the NCIE, with vigorous monsoon and unstable climatic conditions and oscillation between relatively wetter and relatively drier intervals during the NCIE. A cold snap characterized the early Toarcian pre-NCIE interval, as inferred from the increased abundance of microthermic plants. The end of the Jenkyns Event was probably followed by a relatively cooler climate simultaneous with the development of a more temperate forest biome.

The ecological impacts of widespread deforestation during the NCIE were primarily functional losses which led to a more open landscape, with soil erosion, increased runoff and leaching of nutrients and heavy metals that consequently poisoned the terrestrial ecosystem and caused reproductive stress in various plant groups already stressed by climate change. Cheirolepids were probably physiologically better pre-adapted to climatic extremes through their unique reproductive (polyploidy) and/or epidermal features making the group highly resilient during hyperthermal events. Cheirolepidiaceae proliferation is a common marker of rising ambient temperate and extreme weather patterns across Eurasia during the Jenkyns Event. However, the presence of refugia in coastal areas e.g., in NE China suggest spatial differentiation in the vegetation response during and after the Jenkyns Event that was strongly determined by the pre-existing climate gradient and flora.

Funding

This work was funded by the National Natural Science Foundation of China (grant 41888101) and the "WEGETA" internal research project at the Croatian geological survey, funded by the National Recovery and Resilience Plan 2021–2026 of the European Union – NextGenerationEU.

Author contributions

VB and XJ designed the project. VB prepared all the samples and performed the palynological analysis, interpreted the results. All authors discussed the interpretation of the data. VB wrote the text with substantial inputs from XJ, JDC, DBK and comments from BL. DBK acquired the funding.

CRediT authorship contribution statement

Viktória Baranyi: Writing – original draft, Investigation, Formal analysis, Data curation, Conceptualization. **Xin Jin:** Writing – review & editing, Conceptualization. **Jacopo Dal Corso:** Writing – review & editing. **Binbing Li:** Writing – review & editing. **David B. Kemp:** Writing – review & editing, Funding acquisition.

Declaration of competing interest

The authors declare that they have no known competing financial interests or personal relationships that could have appeared to influence the work reported in this paper.

Data availability

The palynological slides are stored in the collections of the Croatian

Geological Survey, Department of Geology, Zagreb, Croatia. Supplementary Material to this article can be found online.

Acknowledgements

We thank reviewers Matías Reolid and Mihai E. Popa for their constructive comments that helped improve the manuscript. This research was conducted within the scope of the internal research project „WEGETA" at the Croatian Geological Survey, funded by the National Recovery and Resilience Plan 2021–2026 of the European Union – NextGenerationEU, and monitored by the Ministry of Science and Education of the Republic of Croatia.". Gilda Lopes (University of Sheffield) is thanked for her help in providing literature on reworked Palaeozoic sporomorphs. We are grateful for Dragica Kovačić (Croatian geological survey) for performing the palynological processing. This work is a contribution to IGCP 739.

Appendix A. Supplementary data

Supplementary data to this article can be found online at https://doi.org/10.1016/j.palaeo.2024.112180.

References

Abbink, O.A., van Konijnenburg-van Cittert, J.H.A., Visscher, H., 2004. A sporomorph ecogroup model for the Northwest European Jurassic – lower cretaceous: concepts and framework. Netherlands J. Geosc. 83, 17–38.

Algeo, T.J., Chen, Z.Q., Fraiser, M.L., Twitchett, R.J., 2011. Terrestrial–marine teleconnections in the collapse and rebuilding of early Triassic marine ecosystems. Palaeogeogr. Palaeocl. 308, 1–11.

Al-Suwaidi, A.H., Ruhk, M., Jenkyns, H.C., Damborenea, S.E., Manceñido, M.O., Condon, D.J., Angelozzi, G.N., Kamo, S.L., Storm, M., Riccardi, A.C., Hesselbo, S.P., 2022. New age constraints on the Lower Jurassic Pliensbachian–Toarcian boundary at Chacay Melehue (Neuquén Basin, Argentina). Sci. Rep. 12, 4975. https://doi.org/10.1038/s41598-022-07886-x.

Arrigo, N., Barker, M.S., 2012. Rarely successful polyploids and their legacy in plant genomes. Curr. Opin. Plant Biol. 15, 140–146.

Ashraf, A.R., Sun, Y., Sun, G., Uhl, D., Mosbrugger, V., Li, J., Herrmann, M., 2010. Triassic and Jurassic palaeoclimate development in the Junggar Basin, Xinjiang, Northwest China—a review and additional lithological data. Palaeobio.Palaeoenv. 90, 187–201.

Axsmith, B.J., 2006. The vegetative structure of a lower cretaceous conifer from Arkansas: further implications for morphospecies concepts in the Cheirolepidiaceae. Cretac. Res. 27, 309–317.

Bailey, T.R., Rosenthal, Y., McArthur, J.M., van de Schootbrugge, B., Thirlwall, M.F., 2003. Paleoceanographic changes of the Late Pliensbachian–Early Toarcian interval: a possible link to the genesis of an Oceanic Anoxic Event. Earth Planet. Sc. Lett. 212, 307–320.

Baker, S.J., Hesselbo, S.P., Lenton, T.M., Duarte, L.V., Belcher, C.M., 2017. Charcoal evidence that rising atmospheric oxygen terminated early Jurassic Ocean anoxia. Nat. Commun. 8, 15018. https://doi.org/10.1038/ncomms15018.

Baranyi, V., Pálfy, J., Görög, Á., Riding, J.B., Raucsik, B., 2016. Multiphase response of palynomorphs to the Toarcian oceanic anoxic event (early Jurassic) in the Réka Valley section, Hungary. Rev. Palaeobot. Palynol. 235, 51–70.

Baranyi, V., Miller, C.S., Ruffell, A., Hounslow, M.W., Kürschner, W.M., 2018. A continental record of the Carnian Pluvial Episode (CPE) from the Mercia Mudstone Group (UK): palynology and climatic. J. Geol. Soc. Lond. 176, 149–166.

Baranyi, V., Jin, X., Dal Corso, J., Shi, Z., Grasby, S.E., Kemp, D.B., 2023. Collapse of terrestrial ecosystems linked to heavy metal poisoning during the Toarcian oceanic anoxic event. Geology 51, 652–656.

Barreda, V.D., Cúneo, N.R., Wilf, P., Currano, E.D., Scasso, R.A., Brinkhuis, H., 2012. Cretaceous/Paleogene floral turnover in Patagonia: drop in diversity, low extinction, and a *Classopollis* spike. PLoS One 7, e52455. https://doi.org/10.1371/journal.pone.0052455.

Batten, D.J., 2002. Palynofacies and petroleum potential. In: Jansonius, J., McGregor, D. C. (Eds.), Palynology: Principles and Applications, vol. 3. American Association of Stratigraphic Palynologists Foundation, pp. 1065–1084.

Belcher, C.M., Mander, L., Rein, G., Jervis, F.X., Haworth, M., Hesselbo, S.P., Glasspool, I. J., McElwain, J.C., 2010. Increased fire activity at the Triassic/Jurassic boundary in Greenland due to climate-driven floral change. Nat. Geosci. 3, 426–429.

Bencha, J.B., Duijnstee, I.A.P., Looy, C.V., 2022. Fossilized pollen malformations as indicators of past environmental stress and meiotic disruption: insights from modern conifers. Paleobiology 48, 677–710.

Betts, R.A., Boucher, O., Collins, M., Cox, P.M., Falloon, P.D., Gedney, N., Hemming, D. L., Huningford, C., Jones, C.D., Sexton, D.M., Web, M.J., 2007. Projected increase in continental runoff due to plant responses to increasing carbon dioxide. Nature 448, 1037–1041.

Birks, H.J.B., 1986. Numerical zonation, comparison and correlation of Quarternary pollen-stratigraphical data. In: Berglund, B.E. (Ed.), Handbook of Holocene Palaeoecology and Palaeohydrology. Wiley & Sons, Chichester, pp. 743–774.

Birks, H.J.B., Birks, H.H., Ammann, B., 2016. The fourth dimension of vegetation. Science 354, 412–413.

Bond, D.P.G., Grasby, S.E., 2017. On the causes of mass extinctions. Palaeogeogr. Palaeocl. 478, 3–29.

Bonis, N., Kürschner, W.M., 2012. Vegetation history, diversity patterns, and climate change across the Triassic/Jurassic boundary. Paleobiology 38, 240–264.

Bonis, N.R., Ruhl, M., Kürschner, W.M., 2010. Milankovitch-scale palynological turnover across the Triassic–Jurassic transition at St. Audrie's Bay, SW UK. J. Geol. Soc. Lond. 167, 877–888.

Bos, R., Lindström, S., van Konijnenburg-van Cittert, H., Hilgen, F., Hollaar, T.P., Aalpoel, H., van der Weijst, C., Sanei, H., Rundra, A., Sluijs, A., van de Schootbrugge, B., 2023. Triassic–Jurassic vegetation response to carbon cycle perturbations and climate change. Glob. Planet. Chang. 228, 104211 https://doi.org/10.1016/j.gloplacha.2023.104211.

Boulila, S., Galbrun, B., Sadki, D., Gardin, S., Bartolini, A., 2019. Constraints on the duration of the early Toarcian T-OAE and evidence for carbon-reservoir change from the High Atlas (Morocco). Glob. Planet. Chang. 175, 113–128.

Bucefalo Palliani, R., 1997. Toarcian sporomorph assemblages from the Umbria-Marche Basin, Central Italy. Palynology 21, 105–121.

Bucefalo Palliani, R., Riding, J.B., 1997. Lower Toarcian palynostratigraphy of Pozzale, Central Italy. Palynology 21, 91–103.

Caruthers, A.H., Smith, P.L., Gröcke, D.R., 2013. The Pliensbachian–Toarcian (Early Jurassic) extinction, a global multi-phased event. Palaeogeogr. Palaeocl. 386, 104–118.

Chandler, M.A., Rind, D., Ruedy, R., 1992. Pangaean climate during the early Jurassic: GCM simulations and the sedimentary record of paleoclimate. Geol. Soc. Am. Bull. 104, 543–559.

Cheng, S., Huang, Y., Fu, X., 1997. Paleogeography reconstruction of the Early-Middle Jurassic large Ordos basin and development and evolution of continental down-warping. Acta Sedimentol. 15, 43–49 (in Chinese with English Abstract).

Chu, D., Dal Corso, J., Shu, W., Haijun, S., Paul, B., Grasby, S.E., van de Schootbrugge, B., Zong, K., Wu, Y., Tong, J., 2021. Metal induced stress in survivor plants following the end-Permian collapse of land ecosystems. Geology 49, 1–5.

Cohen, A.S., Coe, A.L., Harding, S.M., Schwark, L., 2004. Osmium isotope evidence for the regulation of atmospheric CO_2 by continental weathering. Geology 32, 157–160.

Correa-Metrio, A., Dechnik, Y., Lozani-Garcia, S., Caballero, M., 2014. Detrended correspondence analysis: a useful tool to quantify ecological changes from fossil data sets. Bol. Soc. Geol. Mex. 66, 135–143.

Correia, V.F., Riding, J.B., Duarte, L.V., Fernandes, P., Pereira, Z., 2018. The early Jurassic palynostratigraphy of the Lusitanian Basin, western Portugal. Geobios 51, 537–557.

Dejax, J., Pons, D., Yans, J., 2007. Palynology of the dinosaur-bearing Wealden facies in the natural pit of Bernissart (Belgium). Rev. Palaeobot. Palynol. 144, 25–38.

Deng, S.H., Lu, Y.Z., Fan, R., Fang, L.H., Li, X., Liu, L., 2012. Toarcian (early Jurassic) oceanic anoxic event and the responses in terrestrial ecological system. Earth Sci. J. China Univ. Geosci. 37, 23–38 (in Chinese with English abstract).

Deng, S.H., Lu, Y.Z., Zhao, Y., Fan, R., Wang, Y.D., Yang, X.J., Li, X., Sun, B.N., 2017. The Jurassic palaeoclimate regionalization and evolution of China. Earth Sci. Front. 24, 106–142 (In Chinese with English Abstract).

Deng, S.H., Yang, X., Lu, Y., Sha, J., 2024. A thermophilous and arid-tolerant flora from the lower Jurassic of the Junggar Basin, Xinjang, NW China, corresponding to the Toarcian Oceanic Anoxic Event. In: Sha, J., Slater, S.M., Vajda, V., Olsen, P.E., Zhang, H. (Eds.), The Triassic and Jurassic of the Junggar Basin, China: Advances in Palaeontology and Environments, Geological Society, Special Publications, London, vol. 538, pp. 179–210.

Dera, G., Donnadieu, Y., 2012. Modeling evidences for global warming, Arctic seawater freshening, and sluggish oceanic circulation during the early Toarcian anoxic event. Paleoceanography 27, PA211. https://doi.org/10.1029/2012PA002283.

Dera, G., Pellenard, P., Neige, P., Deconick, J.-F., Pucéat, E., Dommergues, J.-L., 2009. Distribution of clay minerals in early Jurassic Peritethyan seas: Palaeoclimatic significance inferred from multiproxy comparisons. Palaeogeogr. Palaeocl. 271, 39–51.

Dera, G., Brigaud, B., Monna, F., Laffont, R., Pucéat, E., Deconick, J.-F., Pellenard, P., Joachimski, M.M., Durlet, C., 2011. Climatic ups and downs in a disturbed Jurassic world. Geology 39, 215–218.

Eberth, D.A., Brinkman, D.B., Chen, P.-J., Yuan, F.-T., Wu, S.-Z., Li, G., Cheng, X.-S., 2001. Sequence stratigraphy, palaeoclimate patterns, and vertebrate fossil preservation in Jurassic-Cretaceous strata of the Junggar Basin, Xinjiang Autonomous Region, People's Republic of China. Can. J. Earth Sci. 38, 1627–1651.

Fantasia, A., Föllmi, K.B., Adatte, T., Bernárdez, E., Spangenberg, J.E., Mattioli, E., 2018. The Toarcian Oceanic Anoxic Event in southwestern Gondwana: an example from the Andean Basin, northern Chile. J. Geol. Soc. Lond. 175, 883–902.

Fay, C.A., 2014. Mid-Cretaceous, pCO_2, Carbon-Cycling and the Rise of the Flowering Plants. PhD thesis,. University College London, pp. 387.

Font, E., Duarte, L.V., Dekkers, M.J., Remazeilles, C., Egli, R., Spangenberg, J.E., Fantasia, A., Ribeiro, J., Gomes, E., Mirão, J., Adatte, T., 2022. Rapid light carbon releases and increased aridity linked to Karoo–Ferrar magmatism during the early Toarcian oceanic anoxic event. Sci. Rep. 12, 4342. https://doi.org/10.1038/s41598-022-08269-y.

Franks, P.J., Beerling, D.J., 2009. CO_2-forced evolution of plant gas exchange capacity and water-use efficiency over the Phanerozoic. Geobiology 7, 227–236.

Galasso, F., Schmid-Röhl, A., Feist-Burkhardt, S., Bernasconi, S.M., Schneebeli-Hermann, E., 2021. Changes in organic matter composition during the Toarcian

Oceanic Anoxic Event (T-OAE) in the Posidonia Shale Formation from Dormettingen (SW-Germany). Palaeogeogr. Palaeocl. 569, 110327 https://doi.org/10.1016/j.palaeo.2021.110327.
Galasso, F., Feist-Burkhardt, S., Schneebeli-Hermann, E., 2022. The palynology of the Toarcian Oceanic Anoxic Event at Dormettingen, Southwest Germany, with emphasis on changes in vegetational dynamics. Rev. Palaeobot. Palynol. 304, 104701 https://doi.org/10.1016/j.revpalbo.2022.104701.
Ge, D.K., Yang, Q., Fu, Z.M., Li, Z., Li, B.F., 1989. The trace fossil and depositional environment of Fuxian Formation, Yulin Country, Northern Shaanxi province. Coal Geol. Explorat. 3, 1–6 (In Chinese with English Abstract).
Ge, D.K., Yang, Q., Fu, Z.M., Li, Z., 1991. The palaeomorphologic features of the basement of the Jurassic coal measures and its control on the sedimentation of Fuxian Formation in Yulin, Shaanxi. Acta Sedimentol. Sin. 9, 65–73 (In Chinese with English Abstract).
Gedney, N., Cox, P.M., Betts, R.A., Boucher, O., Huntingford, C., Stott, P.A., 2006. Detection of a direct carbon dioxide effect in continental river runoff records. Nature 439, 835–838.
Glennie, K.W., Evans, G., 1976. A reconnaissance of the recent sediments of the Ranns of Kutch, India. Sedimentology 23, 625–647.
Gravendyck, J., Schobben, M., Bachelier, J.B., Kürschner, W.M., 2020. Macroecological patterns of the terrestrial vegetation history during the end-Triassic biotic crisis in the central European Basin: a palynological study of the Bonenburg section (NW-Germany) and its supra-regional implications. Glob. Planet. Chang. 194, 103286 https://doi.org/10.1016/j.gloplacha.2020.103286.
Gravendyck, J., Coiffard, C., Bachelier, J.B., Kürschner, W., 2023. Re-evaluation of *Cerebropollenites thiergartii* Eberh.Schulz 1967 and related taxa: priority of *Sciadopityspollenites* and nomenclatural novelties. Grana 62, 1–47.
Grimm, E.C., 1987. CONISS: a FORTRAN 77 program for stratigraphically constrained cluster analysis by the method of incremental sum of squares. Comput. Geosci. 13, 13–35.
Hammer, Ø., Harper, D.A.T., Ryan, P.D., 2001. PAST: Palaeontological statistics software package for education and data analysis. Palaeontol. Electron. 4, 1–9.
Haworth, M., McElwain, J., 2008. Hot, dry, wet, cold or toxic? Revisiting the ecological significance of leaf and cuticular micromorphology. Palaeogeogr. Palaeocl. 262, 79–90.
Helby, R., Morgan, R., Partridge, A.D., 1987. A palynological zonation of the Australian Mesozoic. Mem. Ass. Australas. Palaeontols 4, 1–94.
Hesselbo, S.P., Gröcke, D.R., Jenkyns, H.C., Bjerrum, C.J., Farrimond, P., Bell, H.S.M., Green, O.R., 2000. Massive dissociation of gas hydrate during a Jurassic oceanic anoxic event. Nature 406, 392–395.
Hofmann, C.-C., Odgerel, N., Seyfullah, L.J., 2021. The occurrence of pollen of Sciadopityaceae Luerss. Through time. Fossil Imprint 77, 271–281.
Huang, Z.G., Zhou, H.Q., 1980. Palaeobotany. In: Institute of Geology, Chinese Academy of Geological Sciences (Ed.), Mesozoic Stratigraphy and Palaeontology of Ordos Basin (1). Geological Publishing House, Beijing, pp. 43–114 (in Chinese).
Huang, B.C., Zhou, Y.X., Zhu, R.X., 2008. Discussions on Phanerozoic evolution and formation of continental China, based on paleomagnetic studies. Earth Sci. Front. 15, 348–359 (in Chinese with English abstract).
Jardine, P.E., Harrington, G.I., 2008. The Red Hills Mine Palynoflora: a Diverse Swamp Assemblage from the late Paleocene of Mississippi, U.S.A. Palynology 32, 183–204.
Jenkyns, H.C., 1988. The early Toarcian (Jurassic) Anoxic Event – stratigraphic, sedimentary, and geochemical evidence. Am. J. Sci. 288, 101–151.
Jenkyns, H.C., 2010. Geochemistry of oceanic anoxic events. Geochem. Geophys. Geosyst. 11, Q03004. https://doi.org/10.1029/2009GC002788.
Jin, X., Shi, Z., Baranyi, V., Kemp, D.B., Han, Z., Luo, G., Hu, J., He, F., Chen, L., Preto, N., 2020. The Jenkyns Event (early Toarcian OAE) in the Ordos Basin, North China. Glob. Planet. Chang. 193, 103273 https://doi.org/10.1016/j.gloplacha.2020.103273.
Jin, X., Zhang, F., Baranyi, V., Kemp, D.B., Feng, X., Grasby, S.E., Sun, G., Shi, Z., Chen, W., Dal Corso, J., 2022. Early Jurassic massive release of terrestrial mercury linked to floral crisis. Earth Planet. Sc. Lett. 598, 117842 https://doi.org/10.1016/j.epsl.2022.117842.
Kemp, D.B., Coe, A.L., Cohen, A.S., Schwark, L., 2005. Astronomical pacing of methane release in the early Jurassic period. Nature 437, 396–399.
Kemp, D.B., Baranyi, V., Izumi, K., Burgess, R.D., 2019. Organic matter variations and links to climate across the early Toarcian oceanic anoxic event (T-OAE) in Toyora area, Southwest Japan. Palaeogeogr. Palaeocl. 530, 90–102.
Korte, C., Hesselbo, S.P., Ullmann, C.V., Dietl, G., Ruhl, M., Schweigert, G., Thibault, N., 2015. Jurassic climate mode governed by ocean gateway. Nat. Commun. 6, 10015. https://doi.org/10.1038/ncomms10015.
Kovach, W.L., 1993. Multivariate techniques for biostratigraphical correlation. J. Geol. Soc. Lond. 150, 697–705.
Krencker, F.-N., Bodin, S., Suan, G., Heimhofer, U., Kabiri, L., Immenhauser, A., 2015. Toarcian extreme warmth led to tropical cyclone intensification. Earth Planet. Sc. Lett. 425, 120–130.
Kürschner, W.M., Batenburg, S.J., Mander, L., 2013. Aberrant *Classopollis* pollen reveals evidence for unreduced (2*n*) pollen in the conifer family Cheirolepidiaceae during the Triassic–Jurassic transition. Proc. R. Soc. Lond. B 280, 20131708. https://doi.org/10.1098/rspb.2013.1708.
Levin, D.A., 1983. Polyploidy and novelty in flowering plants. Am. Nat. 122, 1–25.
Li, B.X., Hu, B., 1984. Fossil plants from the Yongdingzhuang Formation of the Datong coalfield, northern Shanxi. Acta Palaeontol. Sin. 23, 135–147.
Li, Y.F., Wang, H., Dilcher, D.L., Bugdaeva, E., Tan, X., Na, Y.L., Sun, C.L., 2019. Middle Jurassic plant diversity and climate in the Ordos Basin, China. Paleontol. J. 53, 1216–1235.
Li, L., Wang, Y.D., Kürschner, W.M., Ruhl, M., Vajda, V., 2020a. Palaeovegetation and palaeoclimate changes across the Triassic–Jurassic transition in the Sichuan Basin, China. Palaeogeogr. Palaeocl. 556, 109891 https://doi.org/10.1016/j.palaeo.2020.109891.
Li, X., Wang, J., Rasbury, T., Zhou, M., Wei, Z., Zhang, C., 2020b. Early Jurassic climate and atmospheric CO_2 concentration in the Sichuan paleobasin, southwestern China. Clim. Past 16, 2055–2074.
Li, B., Jin, X., Dal Corso, J., Ogg, J.G., Lang, X., Baranyi, V., Preto, N., Franceschi, M., Qiao, P., Shi, Z., 2023. Complex pattern of environmental changes and organic matter preservation in the NE Ordos lacustrine depositional system (China) during the T-OAE (early Jurassic). Glob. Planet. Chang. 221, 104045 https://doi.org/10.1016/j.gloplacha.2023.104045.
Lindström, S., 2016. Palynofloral patterns of terrestrial ecosystem change during the end-Triassic event – a review. Geol. Mag. 153, 223–251.
Lindström, S., 2021. Two-phased mass rarity and extinction in land plants during the End-Triassic climate crisis. Front. Earth Sci. 9, 780343 https://doi.org/10.3389/feart.2021.780343.
Lindström, S., Sanei, H., van de Schootbrugge, B., Pedersen, G.K., Lesher, C.E., Tegner, C., Heunisch, C., Dybkjær, K., Outridge, P.M., 2019. Volcanic mercury and mutagenesis in land plants during the end-Triassic mass extinction. Sci. Adv. 5, eaaw4018. https://doi.org/10.1126/sciadv.aaw4018.
Little, C.T.S., Benton, M.J., 1995. Early Jurassic mass extinction: a global long-term event. Geology 23, 495–498.
Liu, M., Zhang, Y.-J., Sun, S.-L., Chen, J.-S., Li, B., Yang, F., Zhang, T., Wang, Y., Wu, Z., 2019. Palynological assemblages of the Beipiao Formation in the Jinyang Basin of western Liaoning, and their age and paleoclimatic significances. Earth Sci. 7, 1–29 (in Chinese).
Loope, D.B., Rowe, C.M., Joeckel, R.M., 2001. Annual monsoon rains recorded by Jurassic dunes. Nature 412, 64–66.
McElwain, J.C., 2018. Paleobotany and global change: important lessons for species to biomes from vegetation responses to past global change. Annu. Rev. Plant Biol. 69, 761–787.
McElwain, J.C., Wade-Murphy, J., Hesselbo, S.P., 2005. Changes in carbon dioxide during an oceanic anoxic event linked to intrusion into Gondwana coals. Nature 435, 479–495.
McElwain, J.C., Popa, M.E., Hesselbo, S.P., Haworth, M., Surlyk, F., 2007. Macroecological responses of terrestrial vegetation to climatic and atmospheric change across the Triassic/Jurassic boundary in East Greenland. Paleobiology 33, 547–573.
Montero-Serrano, J.C., Föllmi, K.B., Adatte, T., Spangenberg, J.E., Tribovillard, N., Fantasia, A., Suan, G., 2015. Continental weathering and redox conditions during the early Toarcian Oceanic Anoxic Event in the northwestern Tethys: insight from the Posidonia Shale section in the Swiss Jura Mountains. Palaeogeogr. Palaeocl. 429, 83–99.
Moore, P.D., Webb, J.A., Collinson, M.E., 1991. Pollen Analysis: Oxford. Blackwell Scientific Publications, 216 pp.
Moulin, M., Fluteau, F., Courtillot, V., Marsh, J., Delpech, G., Quidelleur, X., Gérard, M., 2017. Eruptive history of the Karoo lava flows and their impact on early Jurassic environmental change. J. Geophys. Res. Solid Earth 122, 738–772.
Müller, T., Price, G.D., Bajnai, D., Nyerges, A., Kesjar, D., Raucsik, B., Varga, A., Judik, K., Fekete, J., May, Z., Palfy, J., 2017. New multiproxy record of the Jenkyns Event (also known as the Toarcian Oceanic Anoxic Event) from the Mecsek Mountains (Hungary): differences, duration and drivers. Sedimentology 64, 66–86.
Mussard, J.M., Ducazeaux, J., Cugny, P., 1997. Statistical analyses of Palynomorph Assemblages in Middle Jurassic Deposits (lower to Middle Bathonian, Brent Group, Norway). In: Bull. Des Centres De Recherches Exploration-Production Elf Aquitaine, vol. 21, pp. 265–277.
Nagajyoti, P.C., Lee, K.D., Sreekanth, T.V.M., 2010. Heavy metals, occurrence and toxicity for plants: a review. Environ. Chem. Lett. 8, 199–216.
Nordt, L., Breecker, D., White, J., 2022. Jurassic greenhouse ice-sheet fluctuations sensitive to atmospheric CO_2 dynamics. Nat. Geosci. 15, 54–59.
Olivera, D.E., Zavattieri, A.M., Quattrocchio, M.E., 2015. The palynology of the Cañadón Asfalto Formation (Jurassic), Cerro Cóndor depocentre, Cañadón Asfalto Basin, Patagonia, Argentina: palaeoecology and palaeoclimate based on ecogroup analysis. Palynology 39, 362–386.
Pálfy, J., Smith, P.L., 2000. Synchrony between early Jurassic extinction, oceanic anoxic event, and the Karoo-Ferrar flood basalt volcanism. Geology 28, 747–750.
Paterson, N.W., Mangerud, G., Mørk, A., 2016. Late Triassic (early Carnian) palynology of shallow stratigraphical core 7830/5-U-1, offshore Kong Karls Land, Norwegian Arctic. Palynology 41, 230–254.
Percival, L.M.E., Witt, M.L.I., Mather, T.A., Hermoso, M., Jenkyns, H.C., Hesselbo, S.P., Al-Suwaidi, A.H., Storm, M.S., Xu, W., Ruhl, M., 2015. Globally enhanced mercury deposition during the end-Pliensbachian and Toarcian OAE: a link to the Karoo–Ferrar Large Igneous Province. Earth Planet. Sc. Lett. 428, 267–280.
Peyser, C.E., Poulsen, C.J., 2008. Controls on Permo-Carboniferous precipitation over tropical Pangaea: a GCM sensitivity study. Palaeogeogr. Palaeocl. 268, 181–192.
Pieńkowski, G., Hodbod, M., Ullmann, C.V., 2016. Fungal decomposition of terrestrial organic matter accelerated early Jurassic climate warming. Sci. Rep. 6, 31930. https://doi.org/10.1038/srep31930.
Podani, J., Miklós, I., 2002. Resemblance coefficients and the horseshoe effect in principal coordinates analysis. Ecology 83, 3331–3343.
Pott, C., 2014. A revision of *Wielandiella angustifolia*, a shrub-sized bennettite from the Rhaetian-Hettangian of Scania, Sweden, and Jameson Land, Greenland. Int. J. Plant Sci. 175, 467–499.
Qiu, R., Fang, L., Lv, P., Jiang, F., Zhang, X., Zhang, X., Zhang, P., Zhu, L., Shi, S., 2023. Long eccentricity forcing of the late Pliensbachian to early Toarcian (Jurassic)

terrestrial wildfire activities in the Tarim Basin, northwestern China. Palaeogeogr. Palaeocl. 613, 111408 https://doi.org/10.1016/j.palaeo.2023.111408.
Reiser, R.F., Williams, A.J., 1969. Palynology of the Lower Jurassic sediments of the northern Sural Basin, Queensland. In: Publs. geol. Surv. Qd 339, Palaeonl. Pap., Vol. 15, pp. 1–24.
Reolid, M., Mattioli, E., Duarte, L.V., Marok, A., 2020. The Toarcian Oceanic Anoxic Event and the Jenkyns Event (IGCP-655 final report). Episodes 43. https://doi.org/10.18814/epiiugs/2019/019018.
Reolid, M., Ruebsam, W., Benton, M.J., 2022. Impact of the Jenkyns Event (early Toarcian) on dinosaurs: comparison with the Triassic/Jurassic transition. Earth Sci. Rev. 234, 104196 https://doi.org/10.1016/j.earscirev.2022.104196.
Rodrigues, B., Duarte, L.V., Mendonça Filho, J.G., Santos, L.G., Donizeti de Oliveira, A., 2016. Evidence of terrestrial organic matter deposition across the early Toarcian recorded in the northern Lusitanian Basin, Portugal. Int. J. Coal Geol. 168, 35–45.
Ruebsam, W., Al-Husseini, M., 2020. Calibrating the early Toarcian (early Jurassic) with stratigraphic black holes (SBH). Gondwana Res. 82, 317–336.
Ruebsam, W., Mayer, B., Schwark, L., 2019. Cryosphere carbon dynamics control early Toarcian global warming and sea level evolution. Glob. Planet. Chang. 172, 440–453.
Ruebsam, W., Reolid, M., Sabatino, N., Masetti, D., Schwark, L., 2020a. Molecular paleothermometry of the early Toarcian climate perturbation. Glob. Planet. Chang. 195, 103351 https://doi.org/10.1016/j.gloplacha.2020.103351.
Ruebsam, W., Reolid, M., Schwark, L., 2020b. $\delta^{13}C$ of terrestrial vegetation records Toarcian CO_2 and climate gradients. Sci. Rep. 10, 1–8.
Ruebsam, W., Schmid-Röhl, A., Al-Husseini, M., 2023. Astronomical timescale for the early Toarcian (early Jurassic) Posidonia Shale and global environmental changes. Palaeogeogr. Palaeocl. 623, 11161. https://doi.org/10.1016/j.palaeo.2023.111619.
Sajjadi, F., Playford, G., 2002. Systematic and stratigraphic palynology of the Late Jurassic-earliest Cretaceous strata of the Eromanga Basin, Queesland, Australia. Palaeontogr. Abt. B 261, 1–97.
Sharpe, J., Mehltreter, K., Walker, L., 2010. Ecological importance of ferns. In: Mehltreter, K., Walker, L., Sharpe, J. (Eds.), Fern Ecology. Cambridge University Press, Cambridge, pp. 1–21.
Slater, S.M., Twitchett, R.J., Danise, S., Vajda, V., 2019. Substantial vegetation response to early Jurassic global warming with impacts on oceanic anoxia. Nat. Geosci. 12, 462–467.
Steinthorsdottir, M., Woodward, I., Surlyk, F., McElwain, J.C., 2012. Deep-time evidence of a link between elevated CO_2 concentrations and perturbations in the hydrological cycle via drop in plant transpiration. Geology 40, 815–818.
Suan, G., Pittet, B., Bour, I., Mattioli, E., Duarte, L.V., Mailliot, S., 2008. Duration of the early Toarcian carbon isotope excursion deduced from spectral analysis: consequence for its possible causes. Earth Planet. Sc. Lett. 267, 666–679.
Suan, G., Mattioli, E., Pittet, B., Lécuyer, C., Suchéras-Marx, B., Duarte, L.V., Philippe, M., Reggiani, L., Martineau, F., 2010. Secular environmental precursors to early Toarcian (Jurassic) extreme climate changes. Earth Planet. Sc. Lett. 290, 448–458.
Sun, G., Miao, Y., Mosbrugger, V., Ashraf, A.R., 2010. The Upper Triassic to Middle Jurassic strata and floras of the Junggar Basin, Xinjiang, Northwest China. Palaeobio. Palaeoenv. 90, 203–214.
Them, T.R., Jagoe, C.H., Caruthers, A.H., Gill, B.C., Grasby, S.E., Gröcke, D.R., Yin, R., Owens, J.D., 2019. Terrestrial sources as the primary delivery mechanism of mercury to the oceans across the Toarcian Oceanic Anoxic Event (early Jurassic). Earth Planet. Sc. Lett. 507, 62–72.
Ullmann, C., Boyle, R., Duarte, L., Hesselbo, S.P., Kasemann, S.A., Klein, T.M., Lenton, T. M., Piazza, V., Aberhan, M., 2020. Warm afterglow from the Toarcian Oceanic Anoxic Event drives the success of deep-adapted brachiopods. Sci. Rep. 10, 6549. https://doi.org/10.1038/s41598-020-63487-6.
Vajda, V., McLoughlin, S., Mays, C., Frank, T.D., Fielding, C.R., Tevyaw, A., Lehsten, V., Bocking, M., Nicoll, R.S., 2020. End-Permian (252 Mya) deforestation, wildfires and flooding—an ancient biotic crisis with lessons for the present. Earth Planet. Sc. Lett. 529, 115875 https://doi.org/10.1016/j.epsl.2019.115875.
Vakhrameyev, V.A., 1991. Jurassic and Cretaceous Floras and Climates of the Earth. Cambridge University Press, Cambridge, 340 pp.
van de Schootbrugge, B., Quan, T., Lindström, S., Püttmann, W., Heunisch, C., Pross, J., Fiebig, J., Petschick, R., Röhling, H.-G., Richoz, S., Rosenthal, Y., Falkowski, P.G., 2009. Floral changes across the Triassic/Jurassic boundary linked to flood basalt volcanism. Nat. Geosci. 2, 589–594.
van de Schootbrugge, B., Koutsodendris, A., Taylor, W., Weston, F., Wellman, C., Strother, P.K., 2024. Recognition of an extended record of euglenoid cysts: Implications for the end-Triassic mass extinction. Rev. Palaeobot. Palynol. 322, 105043 https://doi.org/10.1016/j.revpalbo.2023.105043.
van Konijnenburg-Van Cittert, J.H.A., 2002. Ecology of some late Triassic to early cretaceous ferns in Eurasia. Rev. Palaeobot. Palynol. 119, 113–124.
Vannoppen, W., De Baets, S., Keeble, J., Dong, Y., Poesen, J., 2017. How do root and soil characteristics affect the erosion-reducing potential of plant species? Ecol. Eng. 109, 186–195.
Vollmer, T., Werner, R., Weber, M., Tougiannidis, N., Röhling, H.-G., Hambach, U., 2008. Orbital control on Upper Triassic playa cycles of the Steinmergel-Keuper (Norian): a new concept for ancient playa cycles. Palaeogeogr. Palaeocl. 267, 1–16.
Wang, Y.D., 2002. Fern ecological implications from the lower Jurassic in Western Hubei, China. Rev. Palaeobot. Palynol. 119, 125–141.
Wang, Y.D., Mosbrugger, V., Zhang, H., 2005. Early to Middle Jurassic vegetation and climatic events in the Qaidam Basin, Northwest China. Palaeogeogr. Palaeocl. 224, 200–216.
Watson, J., Alvin, K.L., 1996. An English Wealden floral list, with comments on possible environmental indicators. Cretac. Res. 17, 5–26.
Xu, W., Ruhl, M., Jenkyns, H., Hesselbo, S., Riding, J., Selby, D., Naafs, B., Weijers, J., Pancost, R., Tegelaar, E., 2017. Carbon sequestration in an expanding lake system during the Toarcian Oceanic Anoxic Event. Nat. Geosci. 10, 129–135.
Xu, W., Ruhl, M., Jenkyns, H.C., Leng, M.J., Huggett, J.M., Minisini, D., Ullmann, C.V., Riding, J.B., Weijers, J.W.H., Storm, M.S., Percival, L.M.E., Tosca, N.J., Idiz, E.F., Tegelaar, E.W., Hesselbo, S.P., 2018. Evolution of the Toarcian (early Jurassic) carbon-cycle and global climatic controls on local sedimentary processes (Cardigan Bay Basin, UK). Earth Planet. Sc. Lett. 484, 396–411.
Xu, W., Weijers, J.W.H., Ruhl, M., Idiz, E.F., Jenkyns, H.C., Riding, J.B., Gorbanenko, O., Hesselbo, S.P., 2021. Molecular and petrographical evidence for lacustrine environmental and biotic change in the palaeo-Sichuan megalake (China) during the Toarcian Oceanic Anoxic Event. Geol. Soc. Lond. Spec. Publ. 514, 335–357.
Yan, C.F., 1992. The sporo-pollen assemblage from Fuxian formantion in Yulin-Hengshan Region, Shaanxi Province. J. Integr. Plant Biol. 34, 634–640 (In Chinese with English Abstract).
Zakharov, V., Shurygin, B., Ilyna, V., Nikitenko, B., 2006. Pliensbachian-Toarcian biotic turnover in North Siberia and the Arctic region. Stratigr. Geol. Correl. 14, 399–417.
Zhang, Q., Gong, E., Zhang, Y., Guan, C., 2020a. Early Jurassic (Toarcian) warming identified from lacustrine sediments of eastern Liaoning, China. Geol. Mag. 158, 1194–1208.
Zhang, J., Lenz, O.K., Hornung, J., Wang, P., Ebert, M., Hinderer, M., 2020b. Palynology and the Eco-Plant model of peat-forming wetlands of the Upper Triassic Haojiagou Formation in the Junggar Basin, Xinjiang, NW China. Palaeogeogr. Palaeocl. 556, 109888 https://doi.org/10.1016/j.palaeo.2020.109888.
Zhang, J., Lenz, O.K., Wang, P., Hornung, J., 2021. The Eco-Plant model and its implication on Mesozoic dispersed sporomorphs for Bryophytes, Pteridophytes, and Gymnosperms. Rev. Palaeobot. Palynol. 293, 104503 https://doi.org/10.1016/j.revpalbo.2021.104503.
Zhang, Q., Gong, E., Zhang, Y., Guan, C., 2022a. Palynoflora and palaeoclimate of the late early Jurassic (Toarcian) in eastern Liaoning, China. Palaeobio. Palaeoenv. 102, 73–88.
Zhang, P., Lu, J., Yang, M., Bond, D.G., Greene, S.E., Liu, L., Zhang, Y., Wang, Y., Wang, Z., Li, S., Shao, L., Hilton, J., 2022b. Volcanically-induced environmental and floral changes across the Triassic–Jurassic (T–J) transition. Front. Ecol. Evol. 10, 853404 https://doi.org/10.3389/fevo.2022.853404.
Zhang, Y., Mills, B.J.W., He, T., Hu, X., Zhu, M., 2023a. Modeling hyperthermal events in the Mesozoic-Paleogene periods: a review. Front. Ecol. Evol. 11, 1226349. https://doi.org/10.3389/fevo.2023.1226349.
Zhang, P., Yang, M., Lu, J., Jiang, Z., Zhou, K., Liu, H., He, Z., Wang, Y., Bian, X., Shao, L., Hilton, J., Bond, D.P.G., 2023b. Middle Jurassic terrestrial environmental and floral changes linked to volcanism: evidence from the Qinghai-Tibet Plateau, China. Glob. Planet. Chang. 223, 104094 https://doi.org/10.1016/j.gloplacha.2023.104094.